
Understanding and Improving Ensemble Adversarial Defense

Yian Deng

Department of Computer Science
The University of Manchester
Manchester, UK, M13 9PL

yian.deng@manchester.ac.uk

Tingting Mu

Department of Computer Science
The University of Manchester
Manchester, UK, M13 9PL

tingting.mu@manchester.ac.uk

Abstract

The strategy of ensemble has become popular in adversarial defense, which trains multiple base classifiers to defend against adversarial attacks in a cooperative manner. Despite the empirical success, theoretical explanations on why an ensemble of adversarially trained classifiers is more robust than single ones remain unclear. To fill in this gap, we develop a new error theory dedicated to understanding ensemble adversarial defense, demonstrating a provable 0-1 loss reduction on challenging sample sets in adversarial defense scenarios. Guided by this theory, we propose an effective approach to improve ensemble adversarial defense, named interactive global adversarial training (iGAT). The proposal includes (1) a probabilistic distributing rule that selectively allocates to different base classifiers adversarial examples that are globally challenging to the ensemble, and (2) a regularization term to rescue the severest weaknesses of the base classifiers. Being tested over various existing ensemble adversarial defense techniques, iGAT is capable of boosting their performance by up to 17% evaluated using CIFAR10 and CIFAR100 datasets under both white-box and black-box attacks.

1 Introduction

Many contemporary machine learning models, particularly the end-to-end ones based on deep neural networks, admit vulnerabilities to small perturbations in the input feature space. For instance, in computer vision applications, a minor change of image pixels computed by an algorithm can manipulate the classification results to produce undesired predictions, but these pixel changes can be imperceptible to human eyes. Such malicious perturbations are referred to as adversarial attacks. These can result in severe incidents, e.g., medical misdiagnose caused by unauthorized perturbations in medical imaging [46], and wrong actions taken by autonomous vehicles caused by crafted traffic images [37].

The capability of a machine learning model to defend adversarial attacks is referred to as adversarial robustness. A formal way to quantify such robustness is through an adversarial risk, which can be intuitively understood as the expectation of the worst-scenario loss computed within a local neighborhood region around a naturally sampled data example [43]. It is formulated as below:

$$R_{adv}(\mathbf{f}) = \mathbb{E}_{(\mathbf{x}, y) \sim \mathcal{D}} \left[\max_{\mathbf{z} \in \mathcal{B}(\mathbf{x})} \ell(\hat{y}(\mathbf{f}(\mathbf{z})), y) \right], \quad (1)$$

where $\mathcal{B}(\mathbf{x})$ denotes a local neighborhood region around the example \mathbf{x} sampled from a natural data distribution \mathcal{D} . The neighbourhood is usually defined based on a selected norm, e.g., a region containing any \mathbf{z} satisfying $\|\mathbf{z} - \mathbf{x}\| \leq \varepsilon$ for a constant $\varepsilon > 0$. In general, $\ell(\hat{y}, y)$ can be any loss function quantifying the difference between the predicted output \hat{y} and the ground-truth output y . A

learning process that minimizes the adversarial risk is referred to as adversarially robust learning. In the classification context, a way to empirically approximate the adversarial robustness is through a classification error computed using a set of adversarial examples generated by applying adversarial attacks to the model [4]. Here, an adversarial attack refers to an algorithm that usually builds on an optimization strategy, and it produces examples perturbed by a certain strength so that a machine learning model returns the most erroneous output for these examples [10, 27].

On the defense side, there is a rich amount of techniques proposed to improve the model robustness [10, 1]. However, a robust neural network enhanced by a defense technique would mostly result in a reduced accuracy for classifying the natural examples [55]. A relation between the adversarial robustness and the standard accuracy has been formally proved by Tsipras et al. [41]: “*Any classifier that attains at least $1 - \delta$ standard accuracy on a dataset \mathcal{D} has a robust accuracy at most $\delta p / (1 - p)$ against an L_∞ -bounded adversary with $\varepsilon \geq 2\eta$.*”, where ε is the L_∞ bound indicating the attack strength, while η is sufficiently large and $p \geq 0.5$ and they both are used for data generation. This statement presents a tradeoff between the adversarial robustness and natural accuracy. There has been a consistent effort invested to mitigate such tradeoff by developing defense techniques to improve robust accuracy without sacrificing much the natural accuracy.

Ensemble defense has recently arisen as a new state of the art [4, 28]. The core idea is to train strategically multiple base classifiers to defend the attack, with the underlying motivation of improving the statistical stability and cooperation between base models. Existing effort on ensemble defense has mostly been focused on demonstrating performance success for different algorithmic approaches. It is assumed that *training and combining multiple base models can defend better adversarial attacks as compared to training a single model*. Although being supported by empirical success, there is few research that provides rigorous understanding to why this is the case in general. Existing results on analyzing generalized error for ensemble estimators mostly compare the error of the ensemble and the averaged error of the base models, through, for instance, decomposition strategies that divide the error term into bias, variance, co-variance, noise and/or diversity terms [48, 7, 42]. It is not straightforward to extend such results to compare the error of an ensemble model and the error of a model without an ensemble structure.

To address this gap, we develop a new error theory (Theorem 4.1) dedicated to understanding ensemble adversarial defense. The main challenge in mitigating the tradeoff between the adversarial robustness and natural accuracy comes from the fact that adversarial defence techniques can reduce the classifier’s capacity of handling weakly separable example pairs that are close to each other but from different classes. To analyse how ensemble helps address this particular challenge, we derive a provable error reduction by changing from using one neural network to an ensemble of two neural networks through either the average or max combiner of their prediction outputs.

Although ensemble defense can improve the overall adversarial robustness, its base models can still be fooled individually in some input subspaces, due to the nature of the collaborative design. Another contribution we make is the proposal of a simple but effective way to improve each base model by considering the adversarial examples generated by their ensemble accompanied by a regularization term that is designed to recuse the worst base model. We experiment with the proposed enhancement by applying it to improve four state-of-the-art ensemble adversarial defense techniques. Satisfactory performance improvement has been observed when being evaluated using CIFAR-10 and CIFAR-100 datasets [54] under both white-box and black-box attacks.

2 Related Work

Adversarial Attack: Typical attack techniques include white-box and black-box attacks. The white-box adversary has access to the model, e.g., the model parameters, gradients and formulation, etc, while the black-box adversary has limited knowledge of the model, e.g., knowing only the model output, and therefore is closer to the real-world attack setting [5]. Representative white-box attacks include Deepfool [30] and the projected gradient descent (PGD) [29]. The fast gradient sign method (FGSM) [19] is a simplified one-iteration version of PGD. The momentum iterative method (MIM) [15] improves the FGSM attack by introducing the momentum term. Another two commonly-used and cutting-edge white-box attacks are the Carlini-Wagner (CW) attack [8] that computes the perturbation by optimizing the perturbation scales, and the Jacobian-based saliency map attack (JSMA) [34] that perturbs only one pixel in each iteration. Representative black-box attacks include

the square attack (SA) [3], the SignHunter attack [2] and the simple black-box attack (SimBA) [21], among which SA can generate stronger attacks but is more computationally expensive. A thorough survey on adversarial attacks is provided by Akhtar et al. [1]. AutoAttack [12] encapsulates a selected set of strong white and black-box attacks and is considered as the state-of-the-art attack tool. In general, when evaluating the adversarial robustness of a deep learning model, it should be tested under both the white and black-box attacks.

Adversarial Defense: Adversarial training is the most straightforward and commonly used defense technique for improving adversarial robustness. It works by simply expanding the training data with additional adversarial examples. The initial idea was firstly adopted by Christian et al. [11] to train robust neural networks for classification, later on, Madry et al. [29] used adversarial examples generated by the PGD attack for improvement. Overall, this strategy is very adaptive and can be used to defend any attack, but it is on the expense of consuming more training examples. It has been empirically observed that adversarial training can reduce loss curvatures in both the input and model parameter spaces [18, 16], and this reduces the adversarial robustness gap between the training and testing data [55, 50]. These findings motivate the development of a series of regularization techniques for adversarial defense, by explicitly regularizing the curvature or other relevant geometric characteristics of the loss function. Many of these techniques can avoid augmenting the training set and are computationally cheaper. Typical regularization techniques that attempt to flatten the loss surface in the input space include the curvature regularization (CURE) [31], local linearity regularization (LLR) [35], input gradient regularization [32] and Lipschitz regularization [44]. There are also techniques to flatten the loss in the model parameter space, such as TRADES [55], misclassification aware adversarial training (MART) [47], robust self-training (RST) [9, 36], adversarial weight perturbation (AWP) [50], and HAT [49], etc. Alternative to adversarial training and regularization, other defense strategies include pruning [38], pre-training [24], feature denoising [51], domain adaptation [39] and ensemble defense [28, 40], etc. Croce et al. [13] has provided a summary of recent advances.

Ensemble Adversarial Defense: Recently, ensemble has been actively used in adversarial defense, showing promising results. One core spirit behind ensemble is to encourage diversity between base models in order to achieve an improved ensemble prediction [48, 7, 42]. Therefore, the advances are mostly focused on designing effective ensemble diversity losses in training to improve adversarial robustness. For instance, the adaptive diversity promoting (ADP) method [33] uses Shannon entropy for uncertainty regularization and a geometric diversity for measuring the difference between the predictions made by base classifiers. The transferability reduced smooth (TRS) method [53] formulates the diversity term based on cosine similarities between the loss gradients of base models, meanwhile increases the model smoothness via an l_2 -regularization of these gradients during training. The similar idea of exploiting loss gradients was proposed earlier in the gradient alignment loss (GAL) method [26]. The conditional label dependency learning (CLDL) method [45] is a latest improvement over GAL and TRS, which measures the diversity using both the predictions and loss gradients of the base models. However, the ensemble nature of encouraging diversity can cause vulnerability for some base models over certain subsets of adversarial examples [31]. In practice, this can limit the overall robustness of the ensemble when the other base models are not strong enough to correct the weak ones. To address this, the diversifying vulnerabilities for enhanced robust generation of ensembles (DVERGE) [52] proposes a vulnerability diversity to encourage each base model to be robust particularly to the other base models' weaknesses. The latest development for improving ensemble defense, known as synergy-of-experts (SoE) [14], follows a different research path. For each input, it adaptively selects a base model with the largest confidence to make the final prediction instead of combining all, for which the supporting algorithm and theory have been developed. Some surveys on ensemble adversarial attacks and defense can be found in He et al. [23], Lu et al. [28].

3 Notations and Preliminaries

Bold capital and lower-case letters, e.g., \mathbf{X} and \mathbf{x} , denote matrices and vectors, respectively, while lower-case letters, e.g., x , denote scalars. The i -th row and column of a matrix \mathbf{X} are denoted by \mathbf{x}_i and $\mathbf{x}^{(i)}$, respectively, while $x_{i,j}$ and x_i the elements of \mathbf{X} and \mathbf{x} . A classification dataset $D = \{(\mathbf{x}_i, y_i)\}_{i=1}^n$ includes n examples, which are referred to as *natural examples*, with $\mathbf{x}_i \in \mathcal{X} \subset \mathbb{R}^d$ (feature vector) and $y_i \in [C] = \{1, 2, \dots, C\}$ (class label). We sometimes express the label of an example as $y(\mathbf{x})$ or $y_{\mathbf{x}}$. Storing \mathbf{x}_i as a row of $\mathbf{X} \in \mathbb{R}^{n \times d}$ and y_i an element of $\mathbf{y} \in \mathbb{R}^n$, we also denote this dataset by $D = (\mathbf{X}, \mathbf{y})$. The classifier $\mathbf{f} : \mathcal{X} \rightarrow [0, 1]^C$ outputs class probabilities

usually computed by a softmax function. Given the computed probability f_c for the c -th class, $\hat{y}_{\mathbf{f}}(\mathbf{x}) = \arg \max_{c \in [C]} f_c(\mathbf{x})$ predicts the class. For a neural network, we denote by $\mathbf{W}^{(l)}$ the weight matrix connecting the l -th and the $(l - 1)$ -th layers and by $w_{i,j}^{(l)}$ its ij -th element. The L_2 -norm $\|\cdot\|_2$ is used to compute the vector length, while the L_∞ -norm $\|\cdot\|_\infty$ to generate adversarial attacks. Concatenation of two sets is denoted by the symbol \cup .

We focus on classification by minimizing a classification loss $\ell(\mathbf{f}(\mathbf{x}), y_{\mathbf{x}})$, and adapt it to $\ell(\mathbf{f}(\mathbf{X}), \mathbf{y})$ for the whole dataset. Also, we use ℓ_{CE} to emphasize the cross-entropy loss. The loss gradient is $\nabla \ell(\mathbf{f}(\mathbf{x}), y_{\mathbf{x}}) = \frac{\partial \ell(\mathbf{f}(\mathbf{x}), y_{\mathbf{x}})}{\partial \mathbf{x}}$. A cheap way to estimate the loss curvature is by finite difference approximation [31], e.g., the following curvature measure based on L_2 -norm:

$$\lambda_{\mathbf{f}}(\mathbf{x}, \boldsymbol{\delta}) = \frac{\|\nabla \ell(\mathbf{f}(\mathbf{x} + \boldsymbol{\delta}), y_{\mathbf{x}}) - \nabla \ell(\mathbf{f}(\mathbf{x}), y_{\mathbf{x}})\|_2}{\|\boldsymbol{\delta}\|_2}, \quad (2)$$

where $\boldsymbol{\delta} \in \mathbb{R}^d$ is a perturbation. It measures how a surface bends at a point by different amounts in different directions. An adversarial example $\tilde{\mathbf{x}} = \phi(\mathbf{f}, \mathbf{x}, A)$ is generated by attacking the classifier \mathbf{f} using an attack algorithm A on a natural example \mathbf{x} . It is further adapted to $\tilde{\mathbf{X}} = \phi(\mathbf{f}, \mathbf{X}, A)$ for the set of adversarial examples each generated from a natural example in \mathbf{X} . The quantity $\boldsymbol{\delta}(\mathbf{f}, \mathbf{x}, A) = \phi(\mathbf{f}, \mathbf{x}, A) - \mathbf{x}$ is referred to as the *adversarial perturbation* of \mathbf{x} , simplified to $\boldsymbol{\delta}_{\mathbf{x}} = \tilde{\mathbf{x}} - \mathbf{x}$. To control the perturbation strength, we restrict $\|\boldsymbol{\delta}_{\mathbf{x}}\|_\infty \leq \varepsilon$ for some $\varepsilon > 0$, which results in the following adversarial example formulation, as

$$\phi_\varepsilon(\mathbf{f}, \mathbf{x}, A) = \min(\max(\phi(\mathbf{f}, \mathbf{x}, A), \mathbf{x} - \varepsilon), \mathbf{x} + \varepsilon), \quad (3)$$

where both $\min(\cdot, \cdot)$ and $\max(\cdot, \cdot)$ are element-wise operators comparing their inputs.

4 An Error Theory for Adversarial Ensemble Defense

In adversarial ensemble defense, a widely accepted research hypothesis is that training and combining multiple base classifiers can improve adversarial defense as compared to training a single classifier. However, this hypothesis is mostly supported by empirical successes and there is a lack of formal theoretical justification. In this work, we seek theoretical evidence, proving that, when using multi-layer perceptrons (MLPs) for classification, classification error reduces when applying adversarial defence to the base MLPs of an ensemble as compared to a single MLP, under assumptions feasible in practice. The following theorem formalizes our main result.

Theorem 4.1. *Suppose $\mathbf{h}, \mathbf{h}^0, \mathbf{h}^1 \in \mathcal{H} : \mathcal{X} \rightarrow [0, 1]^C$ are C -class L -layer MLPs satisfying Assumption 4.2. Given a dataset $D = \{(\mathbf{x}_i, y_i)\}_{i=1}^n$, construct an ambiguous pair set $A(D)$ by Definition 4.3. Assume $\mathbf{h}, \mathbf{h}^0, \mathbf{h}^1$ are acceptable classifiers for $A(D)$ by Assumption 4.4. Given a classifier $\mathbf{f} \in \mathcal{H} : \mathcal{X} \rightarrow \mathbb{R}^C$ and a dataset D , assess its classification error by 0-1 loss, as*

$$\hat{\mathcal{R}}_{0/1}(D, \mathbf{f}) = \frac{1}{|D|} \sum_{\mathbf{x} \in D} \mathbb{1} \left[f_{y_{\mathbf{x}}}(\mathbf{x}) < \max_{c \neq y_{\mathbf{x}}} f_c(\mathbf{x}) \right], \quad (4)$$

where $\mathbb{1}[\text{true}] = 1$ while $\mathbb{1}[\text{false}] = 0$. For an ensemble $\mathbf{h}_e^{(0,1)}$ of two base MLPs \mathbf{h}^0 and \mathbf{h}^1 through either an average or a max combiner, i.e., $\mathbf{h}_e^{(0,1)} = \frac{1}{2}(\mathbf{h}^0 + \mathbf{h}^1)$ or $\mathbf{h}_e^{(0,1)} = \max(\mathbf{h}^0, \mathbf{h}^1)$, it has a lower empirical 0-1 loss than a single MLP for classifying ambiguous examples, such as

$$\mathbb{E}_{a \sim A(D)} \mathbb{E}_{\mathbf{h}^0, \mathbf{h}^1 \in \mathcal{H}} \left[\hat{\mathcal{R}}_{0/1} \left(a, \mathbf{h}_e^{(0,1)} \right) \right] < \mathbb{E}_{a \sim A(D)} \mathbb{E}_{\mathbf{h} \in \mathcal{H}} \left[\hat{\mathcal{R}}_{0/1} (a, \mathbf{h}) \right]. \quad (5)$$

We prove the result for MLPs satisfying the following assumption.

Assumption 4.2 (MLP Requirement). Suppose a C -class L -layer MLP $\mathbf{h} : \mathbb{R}^d \rightarrow [0, 1]^C$ expressed iteratively by

$$\mathbf{a}^{(0)}(\mathbf{x}) = \mathbf{x}, \quad (6)$$

$$\mathbf{a}^{(l)}(\mathbf{x}) = \sigma \left(\mathbf{W}^{(l)} \mathbf{a}^{(l-1)}(\mathbf{x}) \right), \quad l = 1, 2, \dots, L - 1, \quad (7)$$

$$\mathbf{a}^{(L)}(\mathbf{x}) = \mathbf{W}^{(L)} \mathbf{a}^{(L-1)}(\mathbf{x}) = \mathbf{z}(\mathbf{x}), \quad (8)$$

$$\mathbf{h}(\mathbf{x}) = \text{softmax}(\mathbf{z}(\mathbf{x})), \quad (9)$$

where $\sigma(\cdot)$ is the activation function applied element-wise, the representation vector $\mathbf{z}(\mathbf{x}) \in \mathbb{R}^C$ returned by the L -th layer is fed into the prediction layer building upon the softmax function. Let $w_{s_{l+1}, s_l}^{(l)}$ denote the network weight connecting the s_l -th neuron in the l -th layer and the s_{l+1} -th neuron in the $(l+1)$ -th layer for $l \in \{1, 2, \dots, L\}$. Define a column vector $\mathbf{p}^{(k)}$ with its i -th element computed from the neural network weights and activation derivatives, as $p_i^{(k)} = \sum_{s_L} \frac{\partial a_{s_L}^{(L-1)}(\mathbf{x})}{\partial x_k} w_{i, s_L}^{(L)}$ for $k = 1, 2, \dots, d$ and $i = 1, 2, \dots, C$, also a matrix $\mathbf{P}_h = \sum_{k=1}^d \mathbf{p}^{(k)} \mathbf{p}^{(k)T}$ and its factorization $\mathbf{P}_h = \mathbf{M}_h \mathbf{M}_h^T$ with a full-rank factor matrix \mathbf{M}_h . For constants $\lambda, B > 0$, suppose the following holds for \mathbf{h} :

1. Its cross-entropy loss curvature measured by Eq. (2) satisfies $\lambda_h(\mathbf{x}, \boldsymbol{\delta}) \leq \tilde{\lambda}$.
2. The factor matrix satisfies $\|\mathbf{M}_h\|_2 \leq B_0$ and $\|\mathbf{M}_h^\dagger\|_2 \leq B$, where $\|\cdot\|_2$ denotes the vector induced l_2 -norm for matrix.

We explain the feasibility of the above MLP assumptions in the end of this section.

Although adversarial defense techniques can improve adversarial robustness, new challenges arise in classifying examples that are close to each other but from different classes, due to the flattened loss curvature for reducing the adversarial risk. We refer to a pair of such challenging examples as an *ambiguous pair*. Our strategy of proving improved performance for adversarial defense is to (1) firstly construct a challenging dataset $A(D)$ comprising samples from these pairs, which is referred to as an *ambiguous pair set*, and then (2) prove error reduction over $A(D)$. To start, we provide formal definitions for the ambiguous pair and set.

Definition 4.3 (Ambiguous Pair). Given a dataset $D = \{(\mathbf{x}_i, y_i)\}_{i=1}^n$ where $\mathbf{x}_i \in \mathcal{X}$ and $y_i \in [C]$, an *ambiguous pair* contains two examples $a = ((\mathbf{x}_i, y_i), (\mathbf{x}_j, y_j))$ satisfying $y_i \neq y_j$ and

$$\|\mathbf{x}_i - \mathbf{x}_j\|_2 \leq \frac{1}{JB\sqrt{C(\tilde{\lambda}^2 - \xi)}}, \quad (10)$$

where $J > 2$ is an adjustable control variable, $\tilde{\lambda}$, B and $\xi \leq \tilde{\lambda}^2$ are constants associated with the MLP under Assumption 4.2. The *ambiguous pair set* $A(D)$ contains all the ambiguous pairs existing in D , for which J is adjusted such that $A(D) \neq \emptyset$.

In Theorem 4.1, we are only interested in classifiers that do not fail too badly on $A(D)$, e.g., having an accuracy level above 42.5%. Comparing poorly performed classifiers is not very meaningful, also the studied situation is closer to practical setups where the starting classifiers for improvement are somewhat acceptable. Such a preference is formalized by the following assumption:

Assumption 4.4 (Acceptable Classifier). Suppose an acceptable classifier $\mathbf{f} : \mathbb{R}^d \rightarrow [0, 1]^C$ does not perform poorly on the ambiguous pair set $A(D)$ associated with a control variable J . This means that, for any pair $a = ((\mathbf{x}_i, y_i), (\mathbf{x}_j, y_j)) \in A(D)$ and for any example (\mathbf{x}_i, y_i) from the pair, the following holds:

1. With a probability $p \geq 42.5\%$, the classifier correctly classifies (\mathbf{x}_i, y_i) by a sufficiently large predicted score, i.e., $f_{y_i}(\mathbf{x}_i) \geq 0.5 + \frac{1}{J}$, while wrongly classifies the other example \mathbf{x}_j to y_i by a less score, i.e., $f_{y_i}(\mathbf{x}_j) \leq 0.5 + \frac{1}{J}$.
2. When the classifier predicts (\mathbf{x}_i, y_i) to class \hat{y}_i , the predicted scores for the other classes excluding y_i are sufficiently small, i.e., $f_c(\mathbf{x}_i) \leq \frac{1 - f_{\hat{y}_i}(\mathbf{x}_i)}{C-1}$ for $c \neq y_i, \hat{y}_i$.

Proof for Theorem 4.1 together with a toy illustration example is provided in supplementary material.

Assumption Discussion. Assumption 4.2 is feasible in practice. Reduced loss curvature is a natural result from adversarial defense, particularly for adversarial training and regularization based methods [16, 18] as mentioned in Section 2. Regarding its second part determined by neural network weights and activation derivatives, common training practices like weight regularization and normalization help prevent from obtaining overly inflated elements in \mathbf{P}_h , and thus bound $\|\mathbf{M}_h\|_2$ and $\|\mathbf{M}_h^\dagger\|_2$. Following Definition 4.3, the ambiguous pair $a = ((\mathbf{x}_i, y_i), (\mathbf{x}_j, y_j))$ is constructed to

let the classifier struggle with classifying the neighbouring example, e.g., (\mathbf{x}_j, y_j) , when it is able to classify successfully, e.g., (\mathbf{x}_i, y_i) . Consequently, the success of classifying (\mathbf{x}_i, y_i) is mostly accompanied with a failure of classifying (\mathbf{x}_j, y_j) into y_i , and vice versa. In Assumption 4.4, for an acceptable classifier, the first part assumes its failure is fairly mild, while the second part assumes its struggle is between y_i and y_j . As shown in our proof of Theorem 4.1, in order for Eq. (5) to hold, a polynomial inequality of the probability p needs to be solved, providing a sufficient condition on achieving a reduced ensemble risk, i.e., $p \geq 42.5\%$. Later, we conduct experiments to examine how well some assumptions are met by adversarially trained classifiers and report the results in supplementary material.

5 iGAT: Improving Ensemble Mechanism

Existing ensemble adversarial defense techniques mostly base their design on a framework of combining classification loss and diversity for training. The output of each base classifier contains the probabilities of an example belonging to the C classes. For an input example $\mathbf{x} \in \mathcal{X}$, we denote its output from the i -th base classifier by $\mathbf{h}^i(\mathbf{x}) = [h_1^i(\mathbf{x}), \dots, h_C^i(\mathbf{x})]$ for $i \in [N]$, where N denotes the number of used base classifiers. Typical practice for combining base predictions includes the averaging, i.e., $\mathbf{h}(\mathbf{x}) = \frac{1}{N} \sum_{i=1}^N \mathbf{h}^i(\mathbf{x})$, or the max operation, i.e., $h_j(\mathbf{x}) = \max_{i \in [N]} (h_j^i(\mathbf{x}))$. Without loss of generality, we denote the combiner by $\mathbf{h} = \mathbf{c}(\mathbf{h}^1, \dots, \mathbf{h}^N)$. To train the base classifiers, we exemplify an ensemble loss function using one training example $(\mathbf{x}, y_{\mathbf{x}})$, as below

$$L_E(\mathbf{x}, y_{\mathbf{x}}) = \underbrace{\sum_{i=1}^N \ell(\mathbf{h}^i(\mathbf{x}), y_{\mathbf{x}})}_{\text{classification loss}} + \omega \text{Reg}(\mathbf{h}(\mathbf{x})) + \gamma \text{Diversity}(\mathbf{h}^1(\mathbf{x}), \mathbf{h}^2(\mathbf{x}), \dots, \mathbf{h}^N(\mathbf{x}), y_{\mathbf{x}}), \quad (11)$$

where $\omega, \gamma \geq 0$ are hyperparameters. An example choice for regularization is the Shannon entropy of the ensemble $\mathbf{h}(\mathbf{x})$ [33]. Significant research effort has been invested to diversity design, for which it is optional whether to use the class information in diversity calculation. In the first section of supplementary material, we briefly explain four ensemble adversarial defense techniques highlighting their loss design strategies. These include ADP [33], CLDL [45], DVERGE [52] and SoE [14], and they are used later in Section 6 to test our proposed enhancing approach.

Despite the effort in diversity design that encourages better collaboration between base classifiers, it is unavoidable for some base classifiers to struggle with classifying examples from certain input subspaces. There are intersected subspaces that all the base classifiers are not good at classifying. To address this, we propose an *interactive global adversarial training* (iGAT) approach. It seeks support from adversarial examples globally generated by the ensemble and distributes these examples to base classifiers with a probabilistic strategy empirically proven effective. Additionally, it introduces another regularization term to improve over the severest weakness of the base classifiers. Below we describe our proposal in detail.

5.1 Distributing Global Adversarial Examples

We aim at improving adversarial robustness over intersected feature subspaces which are hard for all base classifiers to classify. These regions can be approximated by global adversarial examples generated by applying adversarial attacks to the ensemble, which are

$$(\tilde{\mathbf{X}}, \tilde{\mathbf{y}}) = (\phi_{\varepsilon}(\mathbf{c}(\mathbf{h}^1, \dots, \mathbf{h}^N), \mathbf{X}, A), \mathbf{y}), \quad (12)$$

where rows of $\tilde{\mathbf{X}}$ store the feature vectors of the generated adversarial examples. For instance, the FGSM attack can be used as A . Instead of feeding the same full set of adversarial examples to train each base classifier, we distribute different examples to different base classifiers, to improve performance and to reduce training time. The generated examples are divided into N groups according to their predicted class probabilities. The i -th group $(\tilde{\mathbf{X}}^i, \tilde{\mathbf{y}}^i)$ is used to train the i -th base classifier, contributing to its classification loss.

Our core distributing strategy is to encourage each base classifier to keep improving over regions that they are relatively good at classifying. This design is motivated by our theoretical result. We have proved in Theorem 4.1 an error reduction achieved by the ensemble of base MLPs that satisfy

the acceptability Assumption 4.4. This assumption is partially examined by whether the classifier returns a sufficiently high prediction score for the correct class or low scores for most of the incorrect classes for some challenging examples. By keeping assigning each base classifier new challenging examples that they are relatively good at classifying, it encourages Assumption 4.4 to continue to hold. In Section 6.3, we perform ablation studies to compare our proposal with a few other distributing strategies, and the empirical results also verify our design. Driven by this strategy, we propose one hard and one soft distributing rule.

Hard Distributing Rule: Given a generated adversarial example $(\tilde{\mathbf{x}}, y) = \left((\tilde{\mathbf{X}})_k, \tilde{y}_k \right)$, the following rule determines which base classifier to assign it:

$$\text{If } h_y^i(\tilde{\mathbf{x}}) > \max_{j \neq i, j \in [N]} h_y^j(\tilde{\mathbf{x}}), \text{ assign } (\tilde{\mathbf{x}}, y) \text{ to } \left(\tilde{\mathbf{X}}^i, \tilde{y}^i \right). \quad (13)$$

We refer to it as a hard distributing rule as it simply assigns examples in a deterministic way. The example is assigned to the base classifier that returns the highest predicted probability on its ground truth class.

Soft Distributing Rule: A hard assignment like the above can be sensitive to errors. Alternatively, we propose a soft distributing rule that utilizes the ranking of the base classifiers based on their prediction performance meanwhile introduces uncertainty. It builds upon roulette wheel selection [6], which is a commonly used genetic operator in genetic algorithms for selecting promising candidate solutions. Firstly, we rank in descending order the predicted probabilities $\{h_y^i(\mathbf{x})\}_{i=1}^N$ by all the base classifiers for the ground truth class, and let $r_x(\mathbf{h}^i) \in [N]$ denote the obtained ranking for the i -th base classifier. Then, we formulate a ranking-based score for each base classifier as

$$p_i = \frac{2^{N-r_x(\mathbf{h}^i)}}{\sum_{i \in [N]} 2^{i-1}}, \quad (14)$$

and it satisfies $\sum_{i \in [N]} p_i = 1$. A more top ranked base classifier has higher score. Next, according to $\{p_i\}_{i=1}^N$, we apply roulette wheel selection and distribute the example to the selected base classifier. Specifically, the selection algorithm constructs N intervals $\{[a_i, b_i]\}_{i=1}^N$ where $a_1 = 0, b_1 = p_1$, also $a_i = b_{i-1}$ and $b_i = a_i + p_i$ for $i = 2, 3, \dots, N$. After sampling a number $q \in (0, 1]$ following a uniform distribution $q \sim U(0, 1)$, check which interval q belongs to. If $a_i < q \leq b_i$, then the example is used to train the i -th base classifier. This enables to assign examples based on ranking but in a probabilistic manner in order to be more robust to errors.

5.2 Regularization Against Misclassification

We introduce another regularization term to address the severest weakness, by minimizing the probability score of the most incorrectly predicted class by the most erroneous base classifier. Given an input example $(\mathbf{x}, y_{\mathbf{x}})$, the proposed term is formulated as

$$L_R(\mathbf{x}, y_{\mathbf{x}}) = -\delta_{0/1}(\mathbf{c}(\mathbf{h}^1(\mathbf{x}), \dots, \mathbf{h}^N(\mathbf{x})), y_{\mathbf{x}}) \log \left(1 - \max_{i=1}^C \max_{j=1}^N h_i^j(\mathbf{x}) \right). \quad (15)$$

Here, $\delta_{0/1}(\mathbf{f}, y) \in \{0, 1\}$ is an error function, where if the input classifier \mathbf{f} can predict the correct label y , it returns 0, otherwise 1. This design is also motivated by Assumption 4.4, to encourage a weak base classifier to perform less poorly on challenging examples so that its chance of satisfying the acceptability assumption can be increased.

5.3 Enhanced Training and Implementation

The proposed enhancement approach iGAT, supported by (1) the global adversarial examples generated and distributed following Section 5.1 and (2) the regularization term proposed in Section 5.2, can be applied to any given ensemble adversarial defense method. We use L_E to denote the original

ensemble loss as in Eq. (11), the enhanced loss for training the base classifiers become

$$\min_{\{\mathbf{h}^i\}_{i=1}^N} \underbrace{\mathbb{E}_{(\mathbf{x}, y_{\mathbf{x}}) \sim (\mathbf{X}, \mathbf{y})} [L_E(\mathbf{x}, y_{\mathbf{x}})]}_{\text{original ensemble loss}} + \underbrace{\alpha \sum_{i=1}^N \mathbb{E}_{(\mathbf{x}, y_{\mathbf{x}}) \sim (\tilde{\mathbf{X}}^i, \tilde{y}^i)} [\ell_{CE}(\mathbf{h}^i(\mathbf{x}), y_{\mathbf{x}})]}_{\text{added global adversarial loss}} + \underbrace{\beta \mathbb{E}_{(\mathbf{x}, y_{\mathbf{x}}) \sim (\mathbf{X}, \mathbf{y}) \cup (\tilde{\mathbf{X}}, \tilde{y})} [L_R(\mathbf{x}, y_{\mathbf{x}})]}_{\text{added misclassification regularization}}, \quad (16)$$

where $\alpha, \beta \geq 0$ are hyper-parameters. In practice, the base classifiers are firstly trained using an existing ensemble adversarial defense technique of interest, i.e., setting $\alpha = \beta = 0$. If some pre-trained base classifiers are available, they can be directly used instead, and fine-tuned with the complete loss. In our implementation, we employ the PGD attack to generate adversarial training examples, as it is the most commonly used in existing literature and in practice.

6 Experiments and Results of iGAT

In the experiments, we compare with six state-of-the-art ensemble adversarial defense techniques including ADP [33], CLDL [45], DVERGE [52], SoE [14], GAL [33] and TRS [53]. The CIFAR-10 and CIFAR-100 datasets are used for evaluation, both containing 50,000 training and 10,000 test images [54]. Overall, ADP, CLDL, DVERGE and SoE appear to be the top performing methods, and we apply iGAT¹ to enhance them. The enhanced, referred to as iGAT_{ADP}, iGAT_{CLDL}, iGAT_{DVERGE} and iGAT_{SoE}, are compared with their original versions, and additionally GAL [33] and TRS [53].

6.1 Experiment Setting

We test against white-box attacks including PGD with 20 inner optimization iterations and CW with L_∞ loss implemented by Wu et al. [50], and the black-box SignHunter (SH) attack [2] with 500 maximum loss queries. In accordance with Carmon et al. [9], the CW attack is applied on 1,000 equidistantly sampled testing examples. We also test against the strongest AutoAttack (AA) [12], which encapsulates variants of the PGD attack and the black-box square attack [3]. All attack methods use the perturbation strength $\varepsilon = 8/255$.

For all the compared methods, an ensemble of $N = 8$ base classifiers with ResNet-20 [22] backbone is experimented, for which results of both the average and max output combiners are reported. To implement the iGAT enhancement, the soft distributing rule from Eq. (14) is used. The two hyper-parameters are set as $\alpha = 0.25$ and $\beta = 0.5$ for SoE, while $\alpha = 5$ and $\beta = 10$ for ADP, CLDL and DVERGE, found by grid search. Here SOE uses a different parameter setting because its loss construction differs from the others, thus it requires a different scale of the parameter range for tuning α and β . In practice, minor adjustments to hyper-parameters have little impact on the results. The iGAT training uses a batch size of 512, and multi-step leaning rates of $\{0.01, 0.002\}$ for CIFAR10 and $\{0.1, 0.02, 0.004\}$ for CIFAR100. Implementation of existing methods uses either their pre-trained models or their source code for training that are publicly available. Each experimental run used one NVIDIA V100 GPU plus 8 CPU cores.

6.2 Result Comparison and Analysis

We compare different defense approaches by reporting their classification accuracies computed using natural images and adversarial examples generated by different attack algorithms, and report the results in Table 1. The proposed enhancement has lifted the performance of ADP and DVERGE to a state-of-the-art level for CIFAR-10 under most of the examined attacks, including both the white-box and black-box ones. The enhanced DVERGE by iGAT has outperformed all the compared methods in most cases for CIFAR-100. In addition, we report in Table 2 the accuracy improvement obtained by iGAT for the studied ensemble defense algorithms, computed as their accuracy difference normalised by the accuracy of the original algorithm. It can be seen that iGAT has positively improved the baseline methods in almost all cases. In many cases, it has achieved an accuracy boost over 10%.

¹The source codes and pre-trained models can be found at <https://github.com/xqsi/iGAT>.

Table 1: Comparison of classification accuracies in percentage reported on natural images and adversarial examples generated by different attack algorithms under L_∞ -norm perturbation strength $\varepsilon = 8/255$. The results are averaged over five independent runs. The best performance is highlighted in bold, the 2nd best underlined.

		Average Combiner (%)					Max Combiner (%)				
		Natural	PGD	CW	SH	AA	Natural	PGD	CW	SH	AA
CIFAR10	TRS	83.15	12.32	10.32	39.21	9.10	82.67	11.89	10.78	37.12	7.66
	GAL	80.85	41.72	41.20	54.94	36.76	80.65	31.95	27.80	50.68	9.26
	SoE	82.19	38.54	37.59	59.69	32.68	82.36	32.51	23.88	41.04	18.37
	iGAT _{SoE}	81.05	40.58	39.65	57.91	34.50	81.19	31.98	24.01	40.67	19.65
	CLDL	84.15	45.32	41.81	55.90	37.04	83.69	39.34	32.80	51.63	15.30
	iGAT _{CLDL}	85.05	<u>45.45</u>	42.00	58.22	37.14	83.73	40.84	34.55	51.70	17.03
	DVERGE	<u>85.12</u>	41.39	43.40	57.33	39.20	<u>84.89</u>	<u>41.13</u>	<u>39.70</u>	54.90	35.15
iGAT _{DVERGE}	85.48	42.53	<u>44.50</u>	57.77	<u>39.48</u>	85.27	42.04	40.70	<u>54.79</u>	35.71	
ADP	82.14	39.63	38.90	52.93	35.53	80.08	36.62	34.60	47.69	27.72	
iGAT _{ADP}	84.96	46.27	44.90	<u>58.90</u>	40.36	80.72	39.37	35.00	48.36	29.83	
CIFAR100	TRS	58.18	10.32	10.12	15.78	6.32	57.21	9.98	9.23	14.21	4.34
	GAL	61.72	22.04	<u>21.60</u>	31.97	<u>18.01</u>	59.39	19.30	13.60	24.73	10.36
	CLDL	58.09	18.47	18.01	29.33	15.52	55.51	18.89	13.07	22.14	4.51
	iGAT _{CLDL}	59.63	18.78	18.20	29.49	14.36	56.91	<u>20.76</u>	14.09	20.43	5.20
	SoE	62.60	20.54	19.60	36.35	15.90	<u>62.62</u>	16.00	11.40	24.25	8.62
	iGAT _{SoE}	63.19	21.89	19.70	<u>35.60</u>	16.16	63.02	16.02	11.45	23.77	8.95
	ADP	60.46	20.97	20.55	30.26	17.37	56.20	17.86	13.70	21.40	10.03
iGAT _{ADP}	60.17	<u>22.23</u>	20.75	30.46	17.88	56.29	17.89	14.10	21.47	10.09	
DVERGE	63.09	20.04	20.01	32.74	17.27	61.20	20.08	<u>15.30</u>	<u>27.18</u>	<u>12.09</u>	
iGAT _{DVERGE}	<u>63.14</u>	23.20	22.50	33.56	18.59	61.54	20.38	17.80	27.88	13.89	

Table 2: Accuracy improvement in percentage by iGAT, i.e. $\frac{iGAT - original}{original} \times 100\%$, reported on natural images and adversarial examples generated by different attack algorithms under L_∞ -norm perturbation strength $\varepsilon = 8/255$.

		Average Combiner					Max Combiner				
		Natural	PGD	CW	SH	AA	Natural	PGD	CW	SH	AA
CIFAR10	ADP	+3.43	+16.75	+15.42	+11.28	+13.59	+0.80	+7.51	+1.16	+1.40	+7.61
	DVERGE	+0.42	+2.75	+2.53	+0.77	+0.71	+0.45	+2.21	+2.52	-0.20	+1.59
	SoE	-1.39	+5.29	+5.48	-2.98	+5.57	-1.42	-1.63	+0.54	-0.90	+6.97
	CLDL	+1.07	+0.29	+0.45	+4.15	+0.27	+0.05	+3.81	+5.34	+0.14	+11.31
CIFAR100	ADP	-0.48	+6.01	+0.97	+0.66	+2.94	+0.16	+0.17	+2.92	+0.33	+0.60
	DVERGE	+0.08	+15.77	+12.44	+2.50	+7.64	+0.56	+1.49	+16.34	+2.58	+14.89
	SoE	+0.94	+6.57	+0.51	-2.06	+1.64	+0.64	+0.13	+0.44	-1.98	+3.83
	CLDL	+2.65	+1.68	+1.05	+0.55	-7.47	+2.52	+9.90	+7.80	-7.72	+15.30

Here are some further discussions on the performance. We observe that DVERGE and its iGAT enhancement perform proficiently on both CIFAR10 and CIFAR100, while ADP and its enhancement are less robust on CIFAR100. We attempt to explain this by delving into the algorithm nature of DVERGE and ADP. The ADP design encourages prediction disparities among the base models. As a result, each base model becomes proficient in classifying a subset of classes that the other base models may struggle with. However, a side effect of this is to discourage base models from becoming good at overlapping classes, which may become ineffective when having to handle a larger number of classes. The reasonably good improvement achieved by iGAT for ADP in Table 2 indicates that an addition of global adversarial examples is able to rescue such situation to a certain extent. On the other hand, in addition to encouraging adversarial diversity among the base models, DVERGE also aims at a stable classification so that each example is learned by multiple base models. This potentially makes it suitable for handling both large and small numbers of classes. Moreover, we also observe that the average combiner provides better performance than the max combiner in general.

Table 3: Results of ablation studies based on $iGAT_{ADP}$ using CIFAR-10 under the PGD attack. The results are averaged over five independent runs. The best performance is highlighted in bold.

	Opposite Distributing	Random Distributing	Hard Distributing	$\beta = 0$	$iGAT_{ADP}$
Natural (%)	82.45	83.05	83.51	83.45	84.96
PGD (%)	41.31	42.60	44.21	42.32	46.25

The reason can be that an aggregated prediction from multiple well-trained base classifiers is more statistically stable.

6.3 Ablation Studies

The key designs of $iGAT$ include its distributing rule and the regularization term. We perform ablation studies to examine their effectiveness. Firstly, we compare the used soft distributing rule with three alternative distributing rules, including (1) a distributing rule opposite to the proposed, which allocates the adversarial examples to the base models that produce the lowest prediction score, (2) a random distributing rule by replacing Eq. (14) by a uniform distribution, and (3) the hard distributing rule in Eq. (13). Then, we compare with the setting of $\beta = 0$ while keeping the others unchanged. This change removes the proposed regularization term. Results are reported in Table 3 using $iGAT_{ADP}$ with the average combiner, evaluated by CIFAR-10 under the PGD attack. It can be seen that a change or removal of a key design results in obvious performance drop, which verifies the effectiveness of the design.

7 Conclusion, Limitation and Future Work

We investigate the challenging and crucial problem of defending against adversarial attacks in the input space of a neural network, with the goal of enhancing ensemble robustness against such attacks while without sacrificing much the natural accuracy. We have provided a formal justification of the advantage of ensemble adversarial defence and proposed an effective algorithmic improvement, bridging the gap between theoretical and practical studies. Specifically, we have proven a decrease in empirical 0-1 loss calculated on data samples challenging to classify, which is constructed to simulate the adversarial attack and defence scenario, under neural network assumptions that are feasible in practice. Also, we have proposed the $iGAT$ approach, applicable to any ensemble adversarial defense technique for improvement. It is supported by (1) a probabilistic distributing rule for selectively allocating global adversarial examples to train base classifiers, and (2) a regularization penalty for addressing vulnerabilities across all base classifiers. We have conducted thorough evaluations and ablation studies using the CIFAR-10 and CIFAR-100 datasets, demonstrating effectiveness of the key designs of $iGAT$. Satisfactory performance improvements up to 17% have been achieved by $iGAT$.

However, there is limitation in our work. For instance, our theoretical result is developed for only two base MLPs. We are in progress of broadening the scope of Theorem 4.1 by further relaxing the neural network assumptions, researching model architectures beyond MLPs and beyond the average/max combiners, and more importantly generalizing the theory to more than two base classifiers. Additionally, we are keen to enrich our evaluations using large-scale datasets, e.g., ImageNet. So far, we focus on exploiting curvature information of the loss landscapes to understand adversarial robustness. In the future, it would be interesting to explore richer geometric information to improve the understanding. Despite the research success, a potential negative societal impact of our work is that it may prompt illegal attackers to develop new attack methods once they become aware of the underlying mechanism behind the ensemble cooperation.

Acknowledgments

We thank the five NeurIPS reviewers for their very insightful and useful comments that help improve the paper draft. We also thank “The University of Manchester - China Scholarship Council Joint Scholarship” for funding Yian’s PhD research.

References

- [1] Naveed Akhtar, Ajmal Mian, Navid Kardan, and Mubarak Shah. Advances in adversarial attacks and defenses in computer vision: A survey. *IEEE Access*, 9:155161–155196, 2021.
- [2] Abdullah Al-Dujaili and Una-May O’Reilly. Sign bits are all you need for black-box attacks. In *International Conference on Learning Representations (ICLR)*, 2020.
- [3] Maksym Andriushchenko, Francesco Croce, Nicolas Flammarion, and Matthias Hein. Square attack: a query-efficient black-box adversarial attack via random search. In *European Conference on Computer Vision (ECCV)*, 2020.
- [4] Tao Bai, Jinqi Luo, Jun Zhao, Bihan Wen, and Qian Wang. Recent advances in adversarial training for adversarial robustness. In *International Joint Conference on Artificial Intelligence (IJCAI)*, pages 4312–4321, 2021.
- [5] Siddhant Bhambri, Sumanyu Muku, Avinash Tulasi, and Arun Balaji Buduru. A survey of black-box adversarial attacks on computer vision models. *arXiv preprint*, 2019.
- [6] Tobias Blickle and Lothar Thiele. A comparison of selection schemes used in evolutionary algorithms. *Evolutionary Computation*, 4(4):361–394, 1996.
- [7] Gavin Brown, Jeremy L Wyatt, Peter Tino, and Yoshua Bengio. Managing diversity in regression ensembles. *Journal of Machine Learning Research (JMLR)*, 6(9), 2005.
- [8] Nicholas Carlini and David Wagner. Towards evaluating the robustness of neural networks. In *IEEE Symposium on Security and Privacy (SP)*, 2017.
- [9] Yair Carmon, Aditi Raghunathan, Ludwig Schmidt, John C Duchi, and Percy S Liang. Unlabeled data improves adversarial robustness. *Advances in neural information processing systems (NeurIPS)*, 32, 2019.
- [10] Anirban Chakraborty, Manaar Alam, Vishal Dey, Anupam Chattopadhyay, and Debdeep Mukhopadhyay. A survey on adversarial attacks and defences. *CAAI Transactions on Intelligence Technology*, 6(1):25–45, 2021.
- [11] Szegedy Christian, Zaremba Wojciech, Sutskever Ilya, Joan Bruna, Dumitru Erhan, Ian J. Goodfellow, and Rob Fergus. Intriguing properties of neural networks. In *International Conference on Learning Representations (ICLR)*, 2014.
- [12] Francesco Croce and Matthias Hein. Reliable evaluation of adversarial robustness with an ensemble of diverse parameter-free attacks. In *International Conference on Machine Learning (ICML)*, 2020.
- [13] Francesco Croce, Maksym Andriushchenko, Vikash Sehwal, Edoardo Debenedetti, Nicolas Flammarion, Mung Chiang, Prateek Mittal, and Matthias Hein. Robustbench: a standardized adversarial robustness benchmark. *arXiv preprint*, 2020.
- [14] Sen Cui, Jingfeng Zhang, Jian Liang, Bo Han, Masashi Sugiyama, and Changshui Zhang. Synergy-of-experts: Collaborate to improve adversarial robustness. *Advances in Neural Information Processing Systems (NeurIPS)*, 35:32552–32567, 2022.
- [15] Yinpeng Dong, Fangzhou Liao, Tianyu Pang, Hang Su, Jun Zhu, Xiaolin Hu, and Jianguo Li. Boosting adversarial attacks with momentum. In *International Conference on Computer Vision and Pattern Recognition (CVPR)*, pages 9185–9193, 2018.
- [16] Alhussein Fawzi, Seyed-Mohsen Moosavi-Dezfooli, Pascal Frossard, and Stefano Soatto. Empirical study of the topology and geometry of deep networks. In *International Conference on Computer Vision and Pattern Recognition (CVPR)*, 2018.
- [17] Gerald B Folland. Higher-order derivatives and Taylor’s formula in several variables. *Preprint*, pages 1–4, 2005.
- [18] C. Daniel Freeman and Joan Bruna. Topology and geometry of half-rectified network optimization. In *International Conference on Learning Representations (ICLR)*, 2017.
- [19] Ian J Goodfellow, Jonathon Shlens, and Christian Szegedy. Explaining and harnessing adversarial examples. *International Conference on Learning Representations (ICLR)*, 2015.
- [20] Biyang Guo, Songqiao Han, Xiao Han, Hailiang Huang, and Ting Lu. Label confusion learning to enhance text classification models. In *The AAAI Conference on Artificial Intelligence (AAAI)*, volume 35, pages 12929–12936, 2021.

- [21] Chuan Guo, Jacob Gardner, Yurong You, Andrew Gordon Wilson, and Kilian Weinberger. Simple black-box adversarial attacks. In *International Conference on Machine Learning (ICML)*, pages 2484–2493, 2019.
- [22] Kaiming He, Xiangyu Zhang, Shaoqing Ren, and Jian Sun. Deep residual learning for image recognition. In *International Conference on Computer Vision and Pattern Recognition (CVPR)*, 2016.
- [23] Ziwen He, Wei Wang, Jing Dong, and Tieniu Tan. Revisiting ensemble adversarial attack. *Signal Processing: Image Communication*, 107:116747, 2022.
- [24] Dan Hendrycks, Kimin Lee, and Mantas Mazeika. Using pre-training can improve model robustness and uncertainty. *International Conference on Machine Learning (ICML)*, 2019.
- [25] Andrew Ilyas, Shibani Santurkar, Dimitris Tsipras, Logan Engstrom, Brandon Tran, and Aleksander Madry. Adversarial examples are not bugs, they are features. *Advances in neural information processing systems (NeurIPS)*, 32, 2019.
- [26] Sanjay Kariyappa and Moinuddin K Qureshi. Improving adversarial robustness of ensembles with diversity training. *arXiv preprint arXiv:1901.09981*, 2019.
- [27] Daniel Lowd and Christopher Meek. Adversarial learning. In *International Conference on Knowledge Discovery and Data Mining (KDD)*, 2005.
- [28] Zhiping Lu, Hongchao Hu, Shumin Huo, and Shuyi Li. Ensemble learning methods of adversarial attacks and defenses in computer vision: Recent progress. In *International Conference on Advanced Computing and Endogenous Security (ACES)*, pages 1–10, 2022.
- [29] Aleksander Madry, Aleksandar Makelov, Ludwig Schmidt, Dimitris Tsipras, and Adrian Vladu. Towards deep learning models resistant to adversarial attacks. In *International Conference on Learning Representations (ICLR)*, 2018.
- [30] Seyed-Mohsen Moosavi-Dezfooli, Alhussein Fawzi, and Pascal Frossard. Deepfool: a simple and accurate method to fool deep neural networks. In *International Conference on Computer Vision and Pattern Recognition CVPR*, 2016.
- [31] Seyed-Mohsen Moosavi-Dezfooli, Alhussein Fawzi, Jonathan Uesato, and Pascal Frossard. Robustness via curvature regularization, and vice versa. In *International Conference on Computer Vision and Pattern Recognition (CVPR)*, 2019.
- [32] Amir Najafi, Shin-ichi Maeda, Masanori Koyama, and Takeru Miyato. Robustness to adversarial perturbations in learning from incomplete data. *Advances in Neural Information Processing Systems (NeurIPS)*, 32, 2019.
- [33] Tianyu Pang, Kun Xu, Chao Du, Ning Chen, and Jun Zhu. Improving adversarial robustness via promoting ensemble diversity. In *International Conference on Machine Learning (ICML)*, pages 4970–4979, 2019.
- [34] Nicolas Papernot, Patrick McDaniel, Somesh Jha, Matt Fredrikson, Z Berkay Celik, and Ananthram Swami. The limitations of deep learning in adversarial settings. In *IEEE European Symposium on Security and Privacy (EuroSP)*, 2016.
- [35] Chongli Qin, James Martens, Sven Gowal, Dilip Krishnan, Krishnamurthy Dvijotham, Alhussein Fawzi, Soham De, Robert Stanforth, and Pushmeet Kohli. Adversarial robustness through local linearization. *Advances in Neural Information Processing Systems (NeurIPS)*, 32, 2019.
- [36] Aditi Raghunathan, Sang M. Xie, Fanny Yang, John C. Duchi, and Percy Liang. Understanding and mitigating the tradeoff between robustness and accuracy. In *International Conference on Machine Learning (ICML)*, 2020.
- [37] Kui Ren, Qian Wang, Cong Wang, Zhan Qin, and Xiaodong Lin. The security of autonomous driving: Threats, defenses, and future directions. *Proceedings of the IEEE*, 108(2):357–372, 2019.
- [38] Vikash Sehwal, Shiqi Wang, Prateek Mittal, and Suman Jana. Hydra: Pruning adversarially robust neural networks. *Advances in Neural Information Processing Systems (NeurIPS)*, 33: 19655–19666, 2020.
- [39] Chuanbiao Song, Kun He, Liwei Wang, and John E. Hopcroft. Improving the generalization of adversarial training with domain adaptation. In *International Conference on Learning Representations (ICLR)*, 2019.

- [40] Florian Tramèr, Alexey Kurakin, Nicolas Papernot, Ian Goodfellow, Dan Boneh, and Patrick McDaniel. Ensemble adversarial training: Attacks and defenses. In *International Conference on Learning Representations (ICLR)*, 2018.
- [41] Dimitris Tsipras, Shibani Santurkar, Logan Engstrom, Alexander Turner, and Aleksander Madry. Robustness may be at odds with accuracy. In *International Conference on Learning Representations (ICLR)*, 2019.
- [42] Naonori Ueda and Ryohei Nakano. Generalization error of ensemble estimators. In *International Conference on Neural Networks (ICNN)*, volume 1, pages 90–95, 1996.
- [43] Jonathan Uesato, Brendan Odonoghue, Pushmeet Kohli, and Aaron Oord. Adversarial risk and the dangers of evaluating against weak attacks. In *International Conference on Machine Learning (ICML)*, 2018.
- [44] Aladin Virmaux and Kevin Scaman. Lipschitz regularity of deep neural networks: analysis and efficient estimation. *Advances in Neural Information Processing Systems (NeurIPS)*, 31, 2018.
- [45] Lele Wang and Bin Liu. Adversarial ensemble training by jointly learning label dependencies and member models. In *International Conference on Intelligent Computing (ICIC)*, pages 3–20, 2023.
- [46] Xianmin Wang, Jing Li, Xiaohui Kuang, Yu-an Tan, and Jin Li. The security of machine learning in an adversarial setting: A survey. *The Journal of Parallel and Distributed Computing (JPDC)*, 130:12–23, 2019.
- [47] Yisen Wang, Difan Zou, Jinfeng Yi, James Bailey, Xingjun Ma, and Quanquan Gu. Improving adversarial robustness requires revisiting misclassified examples. In *International Conference on Learning Representations (ICLR)*, 2019.
- [48] Danny Wood, Tingting Mu, Andrew Webb, Henry Reeve, Mikel Lujan, and Gavin Brown. A unified theory of diversity in ensemble learning. *arXiv preprint arXiv:2301.03962*, 2023.
- [49] Boxi Wu, Jinghui Chen, Deng Cai, Xiaofei He, and Quanquan Gu. Do wider neural networks really help adversarial robustness? *Advances in Neural Information Processing Systems (NeurIPS)*, 34:7054–7067, 2021.
- [50] Dongxian Wu, Shu-Tao Xia, and Yisen Wang. Adversarial weight perturbation helps robust generalization. *Advances in Neural Information Processing Systems (NeurIPS)*, 33:2958–2969, 2020.
- [51] Cihang Xie, Yuxin Wu, Laurens van der Maaten, Alan L Yuille, and Kaiming He. Feature denoising for improving adversarial robustness. In *International Conference on Computer Vision and Pattern Recognition (CVPR)*, 2019.
- [52] Huanrui Yang, Jingyang Zhang, Hongliang Dong, Nathan Inkawhich, Andrew Gardner, Andrew Touchet, Wesley Wilkes, Heath Berry, and Hai Li. Dverge: diversifying vulnerabilities for enhanced robust generation of ensembles. *Advances in Neural Information Processing Systems (NeurIPS)*, 33:5505–5515, 2020.
- [53] Zhuolin Yang, Linyi Li, Xiaojun Xu, Shiliang Zuo, Qian Chen, Pan Zhou, Benjamin Rubinstein, Ce Zhang, and Bo Li. Trs: Transferability reduced ensemble via promoting gradient diversity and model smoothness. *Advances in Neural Information Processing Systems (NeurIPS)*, 34, 2021.
- [54] Sergey Zagoruyko and Nikos Komodakis. Wide residual networks. In *British Machine Vision Conference (BMVC)*, 2016.
- [55] Hongyang Zhang, Yaodong Yu, Jiantao Jiao, Eric Xing, Laurent El Ghaoui, and Michael Jordan. Theoretically principled trade-off between robustness and accuracy. In *International Conference on Machine Learning (ICML)*, 2019.

Appendix

8 Studied Ensemble Adversarial Defense Techniques

We briefly explain four ensemble adversarial defense techniques including ADP [33], CLDL [45], DVERGE [52] and SoE [14]. They are used to test the proposed enhancement approach iGAT. In general, an ensemble model contains multiple base models, and the training is conducted by minimizing their classification losses together with a diversity measure. The output of each base model contains the probabilities of an example belonging to the C classes. For an input example $\mathbf{x} \in \mathcal{X}$, we denote its output from the i -th base classifier by $\mathbf{h}^i(\mathbf{x}) = [h_1^i(\mathbf{x}), \dots, h_C^i(\mathbf{x})]$ for $i \in [N]$, where N denotes the base model number.

8.1 ADP Defense

ADP employs an ensemble by averaging, i.e., $\mathbf{h}(\mathbf{x}) := \frac{1}{N} \sum_{i=1}^N \mathbf{h}^i(\mathbf{x})$. The base classifiers are trained by minimizing a loss that combines (1) the cross entropy loss of each base classifier, (2) the Shannon entropy of the ensemble prediction for regularization, and (3) a diversity measure to encourage different predictions by the base classifiers. Its formulation is exemplified below using one training example $(\mathbf{x}, y_{\mathbf{x}})$:

$$L_{\text{ADP}}(\mathbf{x}, y_{\mathbf{x}}) = \underbrace{\sum_{i=1}^N \ell_{CE}(\mathbf{h}^i(\mathbf{x}), y_{\mathbf{x}})}_{\text{classification loss}} - \underbrace{\alpha H(\mathbf{h}(\mathbf{x}))}_{\text{uncertainty regularization}} + \underbrace{\beta \log(D(\mathbf{h}^1(\mathbf{x}), \mathbf{h}^2(\mathbf{x}), \dots, \mathbf{h}^N(\mathbf{x}), y_{\mathbf{x}}))}_{\text{prediction diversity}}, \quad (17)$$

where $\alpha, \beta \geq 0$ are hyperparameters, the Shannon entropy is $H(\mathbf{p}) = -\sum_{i=1}^C p_i \log(p_i)$, and $D(\mathbf{h}^1, \mathbf{h}^2, \dots, \mathbf{h}^N, y)$ measures the geometric diversity between N different C -dimensional probability vectors. To compute the diversity, a normalized $(C-1)$ -dimensional vector $\tilde{\mathbf{h}}_{\setminus y}^i$ is firstly obtained by removing from \mathbf{h}^i the element at the position $y \in [C]$, the resulting $\{\tilde{\mathbf{h}}_{\setminus y}^i\}_{i=1}^N$ are stored as columns of the $(C-1) \times N$ matrix $\tilde{\mathbf{H}}_{\setminus y}$, and then it has $D(\mathbf{h}^1, \mathbf{h}^2, \dots, \mathbf{h}^N, y) = \det(\tilde{\mathbf{H}}_{\setminus y}^T \tilde{\mathbf{H}}_{\setminus y})$.

8.2 CLDL Defense

CLDL provides an alternative way to formulate the diversity between base classifiers, considering both the base classifier prediction and its loss gradient. Its loss for the training example $(\mathbf{x}, y_{\mathbf{x}})$ is given by

$$L_{\text{CLDL}}(\mathbf{x}, y_{\mathbf{x}}) = \underbrace{\frac{1}{N} \sum_{i=1}^N D_{\text{KL}}(\mathbf{s}^i(\mathbf{x}) || \mathbf{h}^i(\mathbf{x}))}_{\text{classification loss}} - \underbrace{\alpha \log \left(\frac{2}{N(N-1)} \sum_{i=1}^N \sum_{j=i+1}^N e^{\text{JSD}(\mathbf{s}^i(\mathbf{x}) || \mathbf{s}^j(\mathbf{x}))} \right)}_{\text{prediction diversity}} + \underbrace{\frac{2\beta}{N(N-1)} \sum_{i=1}^N \sum_{j=i+1}^N \cos(\nabla D_{\text{KL}}(\mathbf{s}^i(\mathbf{x}) || \mathbf{h}^i(\mathbf{x})), \nabla D_{\text{KL}}(\mathbf{s}^j(\mathbf{x}) || \mathbf{h}^j(\mathbf{x})))}_{\text{gradient diversity}}, \quad (18)$$

where $\mathbf{s}^i(\mathbf{x})$ is a soft label vector computed for $(\mathbf{x}, y_{\mathbf{x}})$ by a label smoothing technique called label confusion model [20]. The vector \mathbf{s}^i is defined as a $(C-1)$ -dimensional vector by removing from \mathbf{s}^i its maximal value. The Kullback–Leibler (KL) divergence is used to examine the difference between the soft label vector and the prediction vector, serving as a soft version of the classification loss. The other used divergence measure is Jensen–Shannon divergence (JSD), given as $\text{JSD}(\mathbf{p} || \mathbf{q}) = \frac{1}{2} (D_{\text{KL}}(\mathbf{p} || \mathbf{g}) + D_{\text{KL}}(\mathbf{q} || \mathbf{g}))$ with $\mathbf{g} = \frac{1}{2}(\mathbf{p} + \mathbf{q})$.

8.3 DVERGE Defense

DVERGE proposes a vulnerability diversity to help training the base classifiers with improved adversarial robustness. For training the i -th base classifier, it minimizes

$$L_{\text{DVERGE}}^{\text{original}}(\mathbf{x}, y_{\mathbf{x}}) = \underbrace{\ell_{\text{CE}}(\mathbf{h}^i(\mathbf{x}), y_{\mathbf{x}})}_{\text{classification loss}} + \alpha \underbrace{\sum_{j \neq i} \mathbb{E}_{(\mathbf{x}_s, y_{\mathbf{x}_s}) \sim D, l \in [L]} \left[\ell_{\text{CE}} \left(\mathbf{h}^i \left(\tilde{\mathbf{x}} \left(\mathbf{h}_{(l)}^j, \mathbf{x}, \mathbf{x}_s \right) \right), y_{\mathbf{x}_s} \right) \right]}_{\text{adversarial vulnerability diversity}}, \quad (19)$$

where $\alpha \geq 0$ is a hyperparameter. Given an input example \mathbf{x} , $\tilde{\mathbf{x}} \left(\mathbf{h}_{(l)}^j, \mathbf{x}, \mathbf{x}_s \right)$ computes its distilled non-robust feature vector proposed by Ilyas et al. [25]. This non-robust feature vector is computed with respect to the l -th layer of the j -th base classifier with its mapping function denoted by $\mathbf{h}_{(l)}^j$ and a randomly sampled natural example \mathbf{x}_s , by

$$\tilde{\mathbf{x}} \left(\mathbf{h}_{(l)}^j, \mathbf{x}, \mathbf{x}_s \right) = \arg \min_{\mathbf{z} \in \mathbb{R}^d} \left\| \mathbf{h}_{(l)}^j(\mathbf{z}) - \mathbf{h}_{(l)}^j(\mathbf{x}) \right\|_2^2, \quad (20)$$

s.t. $\|\mathbf{z} - \mathbf{x}_s\|_{\infty} \leq \epsilon.$

When \mathbf{x} and \mathbf{x}_s belong to different classes, $\tilde{\mathbf{x}}$ can be viewed as an adversarial example that is visually similar to \mathbf{x}_s but is classified by the j -th base classifier into the same class as \mathbf{x} . This represents a weakness of \mathbf{h}^j , and as a correction, the i -th base classifier is trained to correctly classify $\tilde{\mathbf{x}}$ into the same class as \mathbf{x}_s . But when \mathbf{x} and \mathbf{x}_s come from the same class, $(\tilde{\mathbf{x}}, y_{\mathbf{x}_s})$ is just an example similar to the natural one $(\mathbf{x}_s, y_{\mathbf{x}_s}) \in D$, for which the first and second loss terms play similar roles. Therefore, DVERGE simplifies the above loss in practice, and trains each base classifier by

$$\min_{\mathbf{h}^i} L_{\text{DVERGE}}(\mathbf{x}, y_{\mathbf{x}}) = \mathbb{E}_{(\mathbf{x}_s, y_{\mathbf{x}_s}) \sim D, l \in [L]} \left[\sum_{j \neq i} \ell_{\text{CE}} \left(\mathbf{h}^i \left(\tilde{\mathbf{x}} \left(\mathbf{h}_{(l)}^j, \mathbf{x}, \mathbf{x}_s \right) \right), y_{\mathbf{x}_s} \right) \right]. \quad (21)$$

It removes the classification loss on the natural data.

8.4 SoE Defense

SoE proposes a version of classification loss using adversarial examples and a surrogate loss that acts similarly to the vulnerability diversity loss as in DVERGE. For each base classifier \mathbf{h}^i , an auxiliary scalar output head g^i is used to approximate its predicted probability for the true class. Its overall loss exemplified by the training example $(\mathbf{x}, y_{\mathbf{x}})$ is given as

$$L_{\text{SoE}}(\mathbf{x}, y_{\mathbf{x}}) = \underbrace{\sum_{j=1}^N \ell_{\text{BCE}}(h_{y_{\mathbf{x}}}^j(\tilde{\mathbf{x}}^i), g^j(\tilde{\mathbf{x}}^i))}_{\text{adversarial classification loss}} - \sigma \ln \underbrace{\sum_{j=1}^N \exp \left(\frac{-\ell_{\text{CE}}(\mathbf{h}^j(\tilde{\mathbf{x}}^i), y_{\mathbf{x}})}{\sigma} \right)}_{\text{surrogate loss for vulnerability diversity}}, \quad (22)$$

where ℓ_{BCE} is the binary cross entropy loss, and $\sigma > 0$ is the weight parameter. Adversarial examples are generated to compute the losses by using the PGD attack. For the j -th base classifier, the attack is applied to each i -th ($i \neq j$) base classifier to generate training data, resulting in $\tilde{\mathbf{x}}^i = \phi(\mathbf{h}^i, \mathbf{x}, \text{PGD})$. SoE has two training phases and in the second training phase, rather than using $\tilde{\mathbf{x}}^i$, a different adversarial example is generated by $\tilde{\mathbf{x}} = \phi(\mathbf{h}^k, \mathbf{x}, \text{PGD})$ where $k = \arg \max_{i \in [N]} g^i(\mathbf{x})$, aiming at attacking the best-performing base classifier.

9 Proof of Theoretical Results

Given a C -class L -layer MLP $\mathbf{h} : \mathcal{X} \rightarrow [0, 1]^C$ described in Assumption 4.2, we study its cross-entropy loss for one example $(\mathbf{x}, y_{\mathbf{x}})$, i.e., $\ell_{\text{CE}}(\mathbf{h}(\mathbf{x}), y_{\mathbf{x}}) = -\log h_{y_{\mathbf{x}}}(\mathbf{x})$, where its partial derivative with respect to the k -th element of \mathbf{x} is given by

$$\frac{\partial \ell_{\text{CE}}(\mathbf{x})}{\partial x_k} = \sum_{i=1}^C (h_i(\mathbf{x}) - \Delta_{i, y_{\mathbf{x}}}) \frac{\partial z_i}{\partial x_k}, \quad (23)$$

where $\Delta_{i,y_{\mathbf{x}}} = \begin{cases} 1, & \text{if } i = y_{\mathbf{x}}, \\ 0, & \text{otherwise.} \end{cases}$ Perturbing the input \mathbf{x} to $\mathbf{x} + \boldsymbol{\delta}$, sometimes we simplify the notation of the perturbed function output, for instance, $\tilde{\ell}(\mathbf{x}) = \ell(\mathbf{x} + \boldsymbol{\delta})$, $\tilde{\mathbf{h}}(\mathbf{x}) = \mathbf{h}(\mathbf{x} + \boldsymbol{\delta})$, $\tilde{\mathbf{z}}(\mathbf{x}) = \mathbf{z}(\mathbf{x} + \boldsymbol{\delta})$ and $\tilde{\sigma}(\mathbf{x}) = \sigma(\mathbf{x} + \boldsymbol{\delta})$.

Our main theorem builds on a supporting Lemma 9.1. In the lemma, we derive an upper bound for the difference between the predictions $\mathbf{h}(\mathbf{x})$ and $\mathbf{h}(\mathbf{z})$ for two examples, computed by an MLP $\mathbf{h} : \mathbb{R}^d \rightarrow [0, 1]^C$ satisfying Assumption 4.2. Before proceeding to prove the main theorem, we provide a proof sketch. For each ambiguous pair, we firstly analyse its 0/1 risk under different situations when being classified by a single classifier, and derive its empirical 0/1 risk as $r_1 = 1 - p + \frac{1}{2}p^2$. Then we analyse the 0/1 risk for this pair under different situations when being classified by an ensemble classifier, where both max and average combiners are considered. We derive the ensemble empirical 0/1 risk as $r_2 = 1 - 3p^2 + 3p^3 - \frac{3}{4}p^4$. Finally, we prove the main result in Eq. (43) by obtaining a sufficient condition for achieving a reduced ensemble risk, i.e., $p > 0.425$ which enables $r_2 \leq r_1$.

9.1 Lemma 9.1 and Its Proof

Lemma 9.1. *Suppose a C -class L -layer MLP $\mathbf{h} : \mathbb{R}^d \rightarrow [0, 1]^C$ with softmax prediction layer satisfies Assumption 4.2. For any $\mathbf{x}, \mathbf{z} \in \mathbb{R}^d$ and $c = 1, 2, \dots, C$, the following holds*

$$|h_c(\mathbf{x}) - h_c(\mathbf{z})| \leq \|\mathbf{x} - \mathbf{z}\|_2 B \sqrt{C (\tilde{\lambda}^2 - \xi)} \quad (24)$$

for some constant $\xi \leq \tilde{\lambda}^2$, where $\tilde{\lambda}$ and B are constants associated with the MLP family under Assumption 4.2.

Proof. Define the perturbation vector $\boldsymbol{\delta} \in \mathbb{R}^d$ such that $\mathbf{z} = \mathbf{x} + \boldsymbol{\delta}$ and denote its strength by $\epsilon = \|\boldsymbol{\delta}\|_2$, these will be used across the proof. We start from the cross-entropy loss curvature measured by Eq. (2), given as

$$\lambda_{\mathbf{h}}^2(\mathbf{x}, \boldsymbol{\delta}) = \frac{1}{\epsilon^2} \|\nabla \ell_{CE}(\mathbf{h}(\mathbf{x}), y_{\mathbf{x}}) - \ell_{CE}(\mathbf{h}(\mathbf{x} + \boldsymbol{\delta}), y_{\mathbf{x}})\|_2^2 = \frac{1}{\epsilon^2} \sum_k \left(\frac{\partial \ell_{CE}(\mathbf{x})}{\partial x_k} - \frac{\partial \tilde{\ell}_{CE}(\mathbf{x})}{\partial x_k} \right)^2. \quad (25)$$

Below we will expand this curvature expression, where we denote a perturbed function $f(\mathbf{x})$ by using $\tilde{f}(\mathbf{x})$ and $f(\mathbf{x} + \boldsymbol{\delta})$ interchangeably.

By Eq. (23), it has

$$\left| \frac{\partial \ell_{CE}(\mathbf{x})}{\partial x_k} - \frac{\partial \tilde{\ell}_{CE}(\mathbf{x})}{\partial x_k} \right| = \left| \sum_{c=1}^C (h_c(\mathbf{x}) - \Delta_{i,y_{\mathbf{x}}}) \frac{\partial z_i}{\partial x_k} - \sum_{c=1}^C (\tilde{h}_c(\mathbf{x}) - \Delta_{i,y_{\mathbf{x}}}) \frac{\partial \tilde{z}_i}{\partial x_k} \right|. \quad (26)$$

Working with the MLP formulation, it is straightforward to express the quantity $\frac{\partial z_i}{\partial x_k}$ in terms of the derivatives of the activation functions and the neural network weights, as

$$\frac{\partial z_i}{\partial x_k} = \frac{\partial \sum_{s_L} w_{i,s_L}^{(L)} a_{s_L}^{(L-1)}(\mathbf{x})}{\partial x_k} = \sum_{s_L} w_{i,s_L}^{(L)} \frac{\partial a_{s_L}^{(L-1)}(\mathbf{x})}{\partial x_k}. \quad (27)$$

For the convenience of explanation, we simplify the notation by defining $g_{(L-1),s_L}(\mathbf{x}) = \frac{\partial a_{s_L}^{(L-1)}(\mathbf{x})}{\partial x_k}$, and we have

$$\frac{\partial z_i}{\partial x_k} = \sum_{s_L} w_{i,s_L}^{(L)} g_{(L-1),s_L}(\mathbf{x}), \quad (28)$$

$$\frac{\partial \tilde{z}_i}{\partial x_k} = \sum_{s_L} w_{i,s_L}^{(L)} \tilde{g}_{(L-1),s_L}(\mathbf{x}). \quad (29)$$

Applying multivariate Taylor expansion [17], we obtain

$$\tilde{g}_{(L-1),s_L}(\mathbf{x}) = g_{(L-1),s_L}(\mathbf{x}) + \sum_{k=1}^d \frac{\partial g_{(L-1),s_L}(\mathbf{x})}{\partial x_k} \delta_k + \sum_{n \geq 2} \left(\sum_{\substack{a_k \in \mathbb{Z}_0, \\ k \in [d], \\ \sum_{k=1}^d a_k = n}} C_n^{(a_1, \dots, a_d)} \delta_1^{a_1} \dots \delta_d^{a_d} \right), \quad (30)$$

where \mathbb{Z}_0 denotes the set of nonnegative integers, δ_k is the k -th element of the perturbation vector $\boldsymbol{\delta}$, and $C_n^{(a_1, \dots, a_d)}$ denotes the coefficient of each higher-order term of $\delta_1^{a_1} \dots \delta_d^{a_d}$. Combining the above equations, we have

$$\begin{aligned} & \sum_k \left(\frac{\partial \ell_{CE}(\mathbf{x})}{\partial x_k} - \frac{\partial \tilde{\ell}_{CE}(\mathbf{x})}{\partial x_k} \right)^2 \quad (31) \\ &= \sum_k \left(\sum_{i=1}^C \sum_{s_L} \left(h_i(\mathbf{x}) g_{(L-1),s_L}(\mathbf{x}) - \tilde{h}_i(\mathbf{x}) \tilde{g}_{(L-1),s_L}(\mathbf{x}) \right) w_{i,s_L}^{(L)} - \right. \\ & \quad \left. \sum_{s_L} \left(g_{(L-1),s_L}(\mathbf{x}) - \tilde{g}_{(L-1),s_L}(\mathbf{x}) \right) w_{y_{\mathbf{x}},s_L}^{(L)} \right)^2 \\ &= \underbrace{\sum_k \left(\sum_{i=1}^C \sum_{s_L} \left(h_i(\mathbf{x}) - \tilde{h}_i(\mathbf{x}) \right) g_{(L-1),s_L}(\mathbf{x}) w_{i,s_L}^{(L)} \right)^2}_{T(\mathbf{x})} + \underbrace{\sum_{n \geq 1} \left(\sum_{\substack{a_k \in \mathbb{Z}_0, \\ k \in [d], \\ \sum_{k=1}^d a_k = n}} D_n^{(a_1, \dots, a_d)} \delta_1^{a_1} \dots \delta_d^{a_d} \right)^2}_{S(\mathbf{x})}, \end{aligned}$$

where $D_n^{(a_1, \dots, a_d)}$ denotes the coefficient of $\delta_1^{a_1} \dots \delta_d^{a_d}$, computed from the terms like $h_i(\mathbf{x})$, $\tilde{h}_i(\mathbf{x})$, $C_n^{(a_1, \dots, a_d)}$ and the neural network weights. Define a C -dimensional column vector $\mathbf{p}^{(k)}$ with its i -th element computed by $p_i^{(k)} = \sum_{s_L} g_{(L-1),s_L}(\mathbf{x}) w_{i,s_L}^{(L)}$ and a matrix $\mathbf{P}_h = \sum_k \mathbf{p}^{(k)} \mathbf{p}^{(k)T}$, the term $T(\mathbf{x})$ can be rewritten as

$$T(\mathbf{x}) = \sum_k \left(\left(\mathbf{h}(\mathbf{x}) - \tilde{\mathbf{h}}(\mathbf{x}) \right)^T \mathbf{p}^{(k)} \right)^2 = \left(\mathbf{h}(\mathbf{x}) - \tilde{\mathbf{h}}(\mathbf{x}) \right)^T \mathbf{P}_h \left(\mathbf{h}(\mathbf{x}) - \tilde{\mathbf{h}}(\mathbf{x}) \right). \quad (32)$$

The factorization $\mathbf{P}_h = \mathbf{M}_h \mathbf{M}_h^T$ can be obtained by conducting singular value decomposition of \mathbf{P}_h . The above new expression of $T(\mathbf{x})$ helps bound the difference between $\mathbf{h}(\mathbf{x})$ and $\tilde{\mathbf{h}}(\mathbf{x})$.

According to the norm definition, we have

$$\|\mathbf{M}_h\|_2 = \max_{\mathbf{q} \in \mathbb{R}^d \neq \mathbf{0}} \frac{\|\mathbf{M}_h \mathbf{q}\|_2}{\|\mathbf{q}\|_2} = \max_{\mathbf{q} \in \mathbb{R}^C \neq \mathbf{0}} \frac{\|\mathbf{q}^T \mathbf{M}_h\|_2}{\|\mathbf{q}\|_2}, \quad (33)$$

$$\|\mathbf{M}_h^\dagger\|_2 = \max_{\mathbf{q} \in \mathbb{R}^C \neq \mathbf{0}} \frac{\|\mathbf{M}_h^\dagger \mathbf{q}\|_2}{\|\mathbf{q}\|_2} = \max_{\mathbf{q} \in \mathbb{R}^d \neq \mathbf{0}} \frac{\|\mathbf{q}^T \mathbf{M}_h^\dagger\|_2}{\|\mathbf{q}\|_2}. \quad (34)$$

Subsequently, the following holds for any nonzero $\mathbf{q} \in \mathbb{R}^C$ and $\mathbf{p} \in \mathbb{R}^d$

$$\|\mathbf{q}^T \mathbf{M}_h\|_2 \leq \|\mathbf{M}_h\|_2 \|\mathbf{q}\|_2, \quad (35)$$

$$\|\mathbf{p}^T \mathbf{M}_h^\dagger\|_2 \leq \|\mathbf{M}_h^\dagger\|_2 \|\mathbf{p}\|_2. \quad (36)$$

Letting $\mathbf{q} = \mathbf{h}(\mathbf{x}) - \tilde{\mathbf{h}}(\mathbf{x})$ and using the fact that each element in $\mathbf{h}(\mathbf{x})$ and $\tilde{\mathbf{h}}(\mathbf{x})$ is a probability value less than 1, it has

$$T(\mathbf{x}) = \left\| \left(\mathbf{h}(\mathbf{x}) - \tilde{\mathbf{h}}(\mathbf{x}) \right)^T \mathbf{M}_h \right\|_2^2 \leq \|\mathbf{M}_h\|_2^2 \left\| \mathbf{h}(\mathbf{x}) - \tilde{\mathbf{h}}(\mathbf{x}) \right\|_2^2 \leq \left(\sup_{\mathbf{h}} \|\mathbf{M}_h\|_2 \right)^2 C, \quad (37)$$

which results in the fact that $T(\mathbf{x})$ is upper bounded by Assumption 4.2 where $\|\mathbf{M}_h\|_2 \leq B_0$. Letting $\mathbf{p} = \mathbf{M}_h^T (\mathbf{h}(\mathbf{x}) - \tilde{\mathbf{h}}(\mathbf{x}))$ and using the Assumption 4.2 where $\|\mathbf{M}_h^\dagger\|_2 \leq B$, it has

$$\begin{aligned} \|\mathbf{h}(\mathbf{x}) - \tilde{\mathbf{h}}(\mathbf{x})\|_2 &= \left\| \left(\mathbf{h}(\mathbf{x}) - \tilde{\mathbf{h}}(\mathbf{x}) \right)^T \mathbf{M}_h \mathbf{M}_h^\dagger \right\|_2 \\ &\leq \|\mathbf{M}_h^\dagger\|_2 \left\| \left(\mathbf{h}(\mathbf{x}) - \tilde{\mathbf{h}}(\mathbf{x}) \right)^T \mathbf{M}_h \right\|_2 \leq B\sqrt{T(\mathbf{x})}. \end{aligned} \quad (38)$$

Now we focus on analyzing $T(\mathbf{x})$. Working with Eq. (31) and considering the fact that $\sum_k \left(\frac{\partial \ell_{CE}(\mathbf{x})}{\partial x_k} - \frac{\partial \tilde{\ell}_{CE}(\mathbf{x})}{\partial x_k} \right)^2$ is a positive term and $T(\mathbf{x})$ is upper bounded, $S(\mathbf{x})$ has to be lower bounded. We express this lower bound by $\xi\epsilon^2$ using a constant ξ for the convenience of later derivation, resulting in

$$S(\mathbf{x}) \geq \xi\epsilon^2. \quad (39)$$

Given the perturbation strength $\epsilon^2 = \|\boldsymbol{\delta}\|_2^2$, applying the curvature assumption in Assumption 4.2, i.e., $\lambda_h(\mathbf{x}, \boldsymbol{\delta}) \leq \tilde{\lambda}$, also Eqs. (25), (31) and (39), it has

$$T(\mathbf{x}) + \xi\epsilon^2 \leq \tilde{\lambda}^2\epsilon^2 \Rightarrow T(\mathbf{x}) \leq (\tilde{\lambda}^2 - \xi)\epsilon^2. \quad (40)$$

Incorporating this into Eq. (38), it has

$$\|\mathbf{h}(\mathbf{x}) - \tilde{\mathbf{h}}(\mathbf{x})\|_2 \leq \epsilon B \sqrt{\tilde{\lambda}^2 - \xi}. \quad (41)$$

Applying the inequality of $\sum_{i=1}^m a_i^2 \geq \frac{1}{m} \left(\sum_{i=1}^m a_i \right)^2$, also the fact $\sum_{c=1}^C h_c(\mathbf{x}) = \sum_{c=1}^C \tilde{h}_c(\mathbf{x}) = 1$, the following holds for any class $c \in \{1, 2, \dots, C\}$:

$$\begin{aligned} \|\mathbf{h}(\mathbf{x}) - \tilde{\mathbf{h}}(\mathbf{x})\|_2^2 &\geq \sum_{j \neq c} \left| h_j(\mathbf{x}) - \tilde{h}_j(\mathbf{x}) \right|^2 \geq \frac{1}{C-1} \left(\sum_{j \neq c} \left| h_j(\mathbf{x}) - \tilde{h}_j(\mathbf{x}) \right| \right)^2 \\ &\geq \frac{1}{C} \left| \sum_{j \neq c} \left(h_j(\mathbf{x}) - \tilde{h}_j(\mathbf{x}) \right) \right|^2 = \frac{1}{C} \left| h_c(\mathbf{x}) - \tilde{h}_c(\mathbf{x}) \right|^2. \end{aligned} \quad (42)$$

Incorporating Eq. (41) to the above, we have

$$\left| h_c(\mathbf{x}) - \tilde{h}_c(\mathbf{x}) \right| \leq \sqrt{C} \|\mathbf{h}(\mathbf{x}) - \tilde{\mathbf{h}}(\mathbf{x})\|_2 \leq \epsilon B \sqrt{C (\tilde{\lambda}^2 - \xi)}. \quad (43)$$

Inserting back $\mathbf{z} = \mathbf{x} + \boldsymbol{\delta}$ and $\epsilon = \|\boldsymbol{\delta}\|_2$ into Eq. (43), we have

$$\left| h_c(\mathbf{x}) - h_c(\mathbf{z}) \right| \leq \|\mathbf{x} - \mathbf{z}\|_2 B \sqrt{C (\tilde{\lambda}^2 - \xi)}. \quad (44)$$

This completes the proof. □

9.2 Proof of Theorem 4.1

Single Classifier. We analyse the expected 0/1 risk of a single acceptable classifier $\mathbf{h} \in \mathcal{H}$ for a small dataset $D_2 = \{(\mathbf{x}_i, y_i), (\mathbf{x}_j, y_j)\}$ containing the two examples from the ambiguous pair $a = ((\mathbf{x}_i, y_i), (\mathbf{x}_j, y_j))$. The risk is expressed by

$$\mathbb{E}_{\mathbf{h} \in \mathcal{H}} [\hat{\mathcal{R}}_{0/1}(D_2, \mathbf{h})] = \mathbb{E}_{\mathbf{h} \in \mathcal{H}} \left[\frac{1}{2} \left(1 \left[h_{y_i}(\mathbf{x}_i) < \max_{c \neq y_i} h_c(\mathbf{x}_i) \right] + 1 \left[h_{y_j}(\mathbf{x}_j) < \max_{d \neq y_j} h_d(\mathbf{x}_j) \right] \right) \right]. \quad (45)$$

We consider three cases.

Case I: Suppose the example (\mathbf{x}_i, y_i) is correctly classified, thus, according to Assumption 4.4 for acceptable classifiers, it has $h_{y_i}(\mathbf{x}_i) \geq 0.5 + \frac{1}{J}$. As a result, its prediction score for a wrong class ($c \neq y_i$) satisfies

$$h_c(\mathbf{x}_i) \leq 1 - h_{y_i}(\mathbf{x}_i) \leq 1 - (0.5 + \frac{1}{J}) = 0.5 - \frac{1}{J} < 0.5 < h_{y_i}(\mathbf{x}_i). \quad (46)$$

Applying Lemma 9.1 for $c = y_i$ and Eq. (10) in Definition 4.3 for ambiguous pair, it has

$$h_{y_i}(\mathbf{x}_i) - h_{y_i}(\mathbf{x}_j) \leq |h_{y_i}(\mathbf{x}_i) - h_{y_i}(\mathbf{x}_j)| \leq \|\mathbf{x}_i - \mathbf{x}_j\|_2 B \sqrt{C(\tilde{\lambda}^2 - \xi)} \leq \frac{1}{J}. \quad (47)$$

Combining the above with the Case I assumption of $h_{y_i}(\mathbf{x}_i) \geq 0.5 + \frac{1}{J}$, it has

$$h_{y_i}(\mathbf{x}_j) \geq h_{y_i}(\mathbf{x}_i) - \frac{1}{J} \geq (0.5 + \frac{1}{J}) - \frac{1}{J} = 0.5, \quad (48)$$

and hence, for any $c \neq y_i$, it has

$$h_c(\mathbf{x}_j) < 1 - h_{y_i}(\mathbf{x}_j) \leq 0.5 \leq h_{y_i}(\mathbf{x}_j), \quad (49)$$

which indicates that the example (\mathbf{x}_j, y_j) is wrongly predicted to class y_i in Case I. Therefore,

$$\hat{\mathcal{R}}_{0/1}^{(I)}(D_2, \mathbf{h}) = \frac{0+1}{2} = \frac{1}{2}. \quad (50)$$

Case II: Suppose the example (\mathbf{x}_j, y_j) is correctly classified. Following exactly the same derivation as in Case I, this results in the wrong classification of the other example (\mathbf{x}_i, y_i) into class y_j . Therefore,

$$\hat{\mathcal{R}}_{0/1}^{(II)}(D_2, \mathbf{h}) = \frac{1+0}{2} = \frac{1}{2}. \quad (51)$$

Case III: Suppose both examples are misclassified, which simply results in

$$\hat{\mathcal{R}}_{0/1}^{(III)}(D_2, \mathbf{h}) = \frac{1+1}{2} = 1. \quad (52)$$

Note that these three cases are mutually exclusive. Use E_1 , E_2 and E_3 to represent the three events corresponding to Case I, Case II and Case III, respectively. Letting p denote the probability of correctly classifying an example by an acceptable classifier, it is straightforward to obtain $p(E_3) = (1-p)^2$, while $p(E_1) = p(E_2) = \frac{1}{2}(1 - (1-p)^2) = p - \frac{1}{2}p^2$. Therefore, it has

$$\begin{aligned} & \mathbb{E}_{\mathbf{h} \in \mathcal{H}} \left[\hat{\mathcal{R}}_{0/1}(D_2, \mathbf{h}) \right] \\ &= \hat{\mathcal{R}}_{0/1}^{(I)}(D_2, \mathbf{h})p(E_1) + \hat{\mathcal{R}}_{0/1}^{(II)}(D_2, \mathbf{h})p(E_2) + \hat{\mathcal{R}}_{0/1}^{(III)}(D_2, \mathbf{h})p(E_3), \\ &= \frac{1}{2}p(E_1) + \frac{1}{2}p(E_2) + p(E_3) = p - \frac{1}{2}p^2 + (1-p)^2 = 1 - p + \frac{1}{2}p^2. \end{aligned} \quad (53)$$

Ensemble Classifier. We next analyse using D_2 the expected 0/1 risk of an ensemble of two acceptable base classifiers ($\mathbf{h}^0, \mathbf{h}^1 \in \mathcal{H}$) with a *max* or average combiner, in five cases.

Case I: Suppose the example (\mathbf{x}_i, y_i) is correctly classified by both base classifiers. According to Assumption 4.4 for acceptable classifiers, it has $h_{y_i}^0(\mathbf{x}_i) \geq 0.5 + \frac{1}{J}$ and $h_{y_i}^1(\mathbf{x}_i) \geq 0.5 + \frac{1}{J}$. Following exactly the same derivation as in the earlier Case I analysis for a single classifier, i.e., Eqs. (46) and (49), the following holds for any $c \neq y_i$, as

$$h_c^0(\mathbf{x}_i) < h_{y_i}^0(\mathbf{x}_i), \quad h_c^0(\mathbf{x}_j) < h_{y_i}^0(\mathbf{x}_j), \quad (54)$$

$$h_c^1(\mathbf{x}_i) < h_{y_i}^1(\mathbf{x}_i), \quad h_c^1(\mathbf{x}_j) < h_{y_i}^1(\mathbf{x}_j). \quad (55)$$

As a result, for any $c \neq y_i$, the ensemble prediction satisfies the following

$$h_{e,y_i}^{(0,1)}(\mathbf{x}_i) = \max(h_{y_i}^0(\mathbf{x}_i), h_{y_i}^1(\mathbf{x}_i)) > \max(h_c^0(\mathbf{x}_i), h_c^1(\mathbf{x}_i)) = h_{e,c}^{(0,1)}(\mathbf{x}_i), \quad (56)$$

$$h_{e,y_i}^{(0,1)}(\mathbf{x}_i) = \frac{1}{2}(h_{y_i}^0(\mathbf{x}_i) + h_{y_i}^1(\mathbf{x}_i)) > \frac{1}{2}(h_c^0(\mathbf{x}_i) + h_c^1(\mathbf{x}_i)) = h_{e,c}^{(0,1)}(\mathbf{x}_i), \quad (57)$$

each corresponding to the max and average combiners, respectively. This indicates a correct ensemble classification of (\mathbf{x}_i, y_i) . Also, it satisfies

$$h_{e,y_j}^{(0,1)}(\mathbf{x}_j) = \max(h_{y_j}^0(\mathbf{x}_j), h_{y_j}^1(\mathbf{x}_j)) < \max(h_{y_i}^0(\mathbf{x}_j), h_{y_i}^1(\mathbf{x}_j)) = h_{e,y_i}^{(0,1)}(\mathbf{x}_j), \quad (58)$$

$$h_{e,y_j}^{(0,1)}(\mathbf{x}_j) = \frac{1}{2} (h_{y_j}^0(\mathbf{x}_j) + h_{y_j}^1(\mathbf{x}_j)) < \frac{1}{2} (h_{y_i}^0(\mathbf{x}_j) + h_{y_i}^1(\mathbf{x}_j)) = h_{e,y_i}^{(0,1)}(\mathbf{x}_j), \quad (59)$$

when using the max and average combiners, respectively. This indicates a wrong classification of (\mathbf{x}_j, y_j) . Finally, for Case I, we have

$$\hat{\mathcal{R}}_{0/1}^{(I)}(D_2, \mathbf{h}_e^{(0,1)}) = \frac{1}{2} (0 + 1) = \frac{1}{2}, \quad (60)$$

Case II: Suppose the example (\mathbf{x}_j, y_j) is correctly classified by both base classifiers. By following exactly the same derivation as in Case I as above, the ensemble correctly classifies (\mathbf{x}_j, y_j) , while wrongly classifies (\mathbf{x}_i, y_i) . As a result, it has

$$\hat{\mathcal{R}}_{0/1}^{(II)}(D_2, \mathbf{h}_e^{(0,1)}) = \frac{1}{2} (1 + 0) = \frac{1}{2}. \quad (61)$$

Case III: Suppose the example (\mathbf{x}_i, y_i) is correctly classified by \mathbf{h}^0 , while the other example (\mathbf{x}_j, y_j) is correctly classified by \mathbf{h}^1 , i.e., $h_{y_i}^0(\mathbf{x}_i) \geq 0.5 + \frac{1}{J}$ and $h_{y_j}^1(\mathbf{x}_j) \geq 0.5 + \frac{1}{J}$ according to Assumption 4.4. Following a similar analysis as in Case I for a single classifier, we know that \mathbf{h}^0 consequently misclassifies (\mathbf{x}_j, y_j) into y_i , while \mathbf{h}^1 misclassifies (\mathbf{x}_i, y_i) into y_j . Also, by Assumption 4.4, it is assumed that the misclassification happens with a less score than $0.5 + \frac{1}{J}$, thus, $h_{y_i}^0(\mathbf{x}_j) \leq 0.5 + \frac{1}{J}$ and $h_{y_j}^1(\mathbf{x}_i) \leq 0.5 + \frac{1}{J}$. Combining all these, for any $c \neq y_i$ and $d \neq y_j$, we have

$$h_d^1(\mathbf{x}_i) < 0.5 \leq h_{y_j}^1(\mathbf{x}_i) \leq 0.5 + \frac{1}{J} \leq h_{y_i}^0(\mathbf{x}_i), \quad (62)$$

$$h_c^0(\mathbf{x}_j) < 0.5 \leq h_{y_i}^0(\mathbf{x}_j) \leq 0.5 + \frac{1}{J} \leq h_{y_j}^1(\mathbf{x}_j), \quad (63)$$

and according to the second condition in Assumption 4.4, it has

$$h_c^0(\mathbf{x}_i) \leq \frac{1 - h_{y_i}^0(\mathbf{x}_i)}{C - 1} \leq h_{y_i}^0(\mathbf{x}_i), \quad (64)$$

$$h_d^1(\mathbf{x}_j) \leq \frac{1 - h_{y_j}^1(\mathbf{x}_j)}{C - 1} \leq h_{y_j}^1(\mathbf{x}_j). \quad (65)$$

Subsequently, the ensemble prediction by a max combiner satisfies

$$h_{e,y_i}^{(0,1)}(\mathbf{x}_i) = \max(h_{y_i}^0(\mathbf{x}_i), h_{y_i}^1(\mathbf{x}_i)) = h_{y_i}^0(\mathbf{x}_i) > \max(h_c^0(\mathbf{x}_i), h_c^1(\mathbf{x}_i)) = h_{e,c}^{(0,1)}(\mathbf{x}_i), \quad (66)$$

$$h_{e,y_j}^{(0,1)}(\mathbf{x}_j) = \max(h_{y_j}^0(\mathbf{x}_j), h_{y_j}^1(\mathbf{x}_j)) = h_{y_j}^1(\mathbf{x}_j) > \max(h_d^0(\mathbf{x}_j), h_d^1(\mathbf{x}_j)) = h_{e,d}^{(0,1)}(\mathbf{x}_j), \quad (67)$$

which indicates a correct classification of both examples.

Now we consider the slightly more complex situation of ensemble by averaging. According to the previous analysis, we know that \mathbf{x}_i is classified by \mathbf{h}^1 to y_j , and \mathbf{x}_j is classified by \mathbf{h}^0 to y_i . Applying the second condition in Assumption 4.4, we analyse the quantity $1 - h_{y_j}^1(\mathbf{x}_i) - h_{y_i}^0(\mathbf{x}_j)$ as

$$1 - h_{y_j}^1(\mathbf{x}_i) - h_{y_i}^0(\mathbf{x}_j) = \sum_{c \neq y_i, y_j} h_c^1(\mathbf{x}_i) \leq (C - 2) \frac{1 - h_{y_j}^1(\mathbf{x}_i)}{C - 1} = 1 - h_{y_j}^1(\mathbf{x}_i) - \left(\frac{1 - h_{y_j}^1(\mathbf{x}_i)}{C - 1} \right), \quad (68)$$

resulting in

$$h_{y_i}^1(\mathbf{x}_i) \geq \frac{1 - h_{y_j}^1(\mathbf{x}_i)}{C - 1}. \quad (69)$$

Combining Eq. (62), Eq. (64) and Eq. (69), it has

$$h_{y_i}^1(\mathbf{x}_i) \geq \frac{1 - h_{y_j}^1(\mathbf{x}_i)}{C - 1} > \frac{1 - h_{y_i}^0(\mathbf{x}_i)}{C - 1} \geq h_c^0(\mathbf{x}_i). \quad (70)$$

On the other hand, from Eq. (62), one can obtain

$$h_{y_i}^0(\mathbf{x}_i) \geq h_c^1(\mathbf{x}_i). \quad (71)$$

As a result, the ensemble prediction by an average combiner satisfies

$$h_{e,y_i}^{(0,1)}(\mathbf{x}_i) = \frac{1}{2} (h_{y_i}^0(\mathbf{x}_i) + h_{y_i}^1(\mathbf{x}_i)) > \frac{1}{2} (h_c^0(\mathbf{x}_i) + h_c^1(\mathbf{x}_i)) = h_{e,c}^{(0,1)}(\mathbf{x}_i), \quad (72)$$

for any $c \neq y_i$. Following the same way of deriving Eqs. (70) and (71), but for \mathbf{x}_j , we can obtain another two inequalities $h_{y_j}^1(\mathbf{x}_j) \geq h_d^0(\mathbf{x}_j)$ and $h_{y_j}^0(\mathbf{x}_j) \geq h_d^1(\mathbf{x}_j)$, for any $d \neq y_j$, and subsequently,

$$h_{e,y_j}^{(0,1)}(\mathbf{x}_j) = \frac{1}{2} (h_{y_j}^0(\mathbf{x}_j) + h_{y_j}^1(\mathbf{x}_j)) > \frac{1}{2} (h_d^0(\mathbf{x}_j) + h_d^1(\mathbf{x}_j)) = h_{e,d}^{(0,1)}(\mathbf{x}_j). \quad (73)$$

Putting together Eqs. (72) and (73), a correct ensemble classification is achieved for both examples. Finally, we conclude the following result

$$\hat{\mathcal{R}}_{0/1}^{(\text{III})} (D_2, \mathbf{h}_e^{(0,1)}) = 0, \quad (74)$$

which is applicable to both the max and average combiners.

Case IV: Suppose the example (\mathbf{x}_i, y_i) is correctly classified by \mathbf{h}^1 while the other example (\mathbf{x}_j, y_j) is correctly classified by \mathbf{h}^0 . This is essentially the same situation as in Case III, and the same result $\hat{\mathcal{R}}_{0/1}^{(\text{IV})} (D_2, \mathbf{h}_e^{(0,1)}) = 0$ is obtained.

Case V: This case represents all the remaining situations, where, for instance, the example (\mathbf{x}_i, y_i) and/or (\mathbf{x}_j, y_j) is misclassified by both base classifiers. Here, we do not have sufficient information to analyse the error in detail, and also it is not necessary to do so for our purpose. So we just simply leave it as $\hat{\mathcal{R}}_{0/1}^{(\text{V})} (D_2, \mathbf{h}_e^{(0,1)}) \leq 1$.

These five cases are mutually exclusive, and we use $\{H_i\}_{i=1}^5$ to denote them accordingly. The first four cases represent the same situation that each example is correctly classified by a single base classifier, therefore $p(H_1) = p(H_2) = p(H_3) = p(H_4) = p(E_1)p(E_2) = (p - \frac{1}{2}p^2)^2$, while $p(H_5) = 1 - \sum_{i=1}^4 p(H_i) = 1 - 4(p - \frac{1}{2}p^2)^2 = 1 - (2p - p^2)^2$. Incorporating the result of $\hat{\mathcal{R}}_{0/1} (D_2, \mathbf{h}_e^{(0,1)})$ regarding to the five cases, we have

$$\begin{aligned} & \mathbb{E}_{\mathbf{h}^0, \mathbf{h}^1 \in \mathcal{H}} \left[\hat{\mathcal{R}}_{0/1} (D_2, \mathbf{h}_e^{(0,1)}) \right] \\ & \leq \frac{1}{2}p(H_1) + \frac{1}{2}p(H_2) + 0(p(H_3) + p(H_4)) + p(H_5) \\ & = \left(p - \frac{1}{2}p^2 \right)^2 + 1 - (2p - p^2)^2 = 1 - 3p^2 + 3p^3 - \frac{3}{4}p^4. \end{aligned} \quad (75)$$

Risk Comparison. We examine the sufficient condition for achieving a reduced ensemble loss for this dataset D_2 , i.e.,

$$\mathbb{E}_{\mathbf{h}^0, \mathbf{h}^1 \in \mathcal{H}} \left[\hat{\mathcal{R}}_{0/1} (D_2, \mathbf{h}_e^{(0,1)}) \right] < \mathbb{E}_{\mathbf{h} \in \mathcal{H}} \left[\hat{\mathcal{R}}_{0/1} (D_2, \mathbf{h}) \right]. \quad (76)$$

Incorporating Eqs. (53) and (75), this requires to solve the following polynomial inequality, as

$$1 - 3p^2 + 3p^3 - \frac{3}{4}p^4 < 1 - p + \frac{1}{2}p^2, \quad (77)$$

for which $p > 0.425$ provides a solution. Applying the expectation $\mathbb{E}_{a \sim A(D)}$ over the data samples, where the ambiguous pair a is equivalent to D_2 , Eq. (5) from the theorem is obtained. This completes the proof.

10 A Toy Example for Theorem 4.1

Guided by Theorem 4.1, we aim to verify the difference between the single-branch and ensemble mechanisms using 1-dimensional 2-class data. Suppose $D = \{(\mathbf{x}_i = 0.3, y_i = 0), (\mathbf{x}_j = 0.7, y_j =$

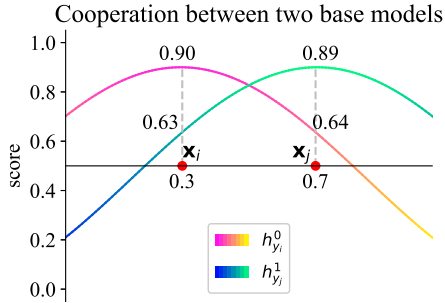


Figure 1: Illustration for Theorem 4.1.

Table 4: Results on two additional black-box attacks.

	Simple Attack (%)	Bandits Attack (%)
ADP	75.91	59.21
iGAT _{ADP}	79.43	64.55
DVERGE	79.43	63.80
iGAT _{DVERGE}	79.61	64.89
CLDL	76.82	63.80
iGAT _{CLDL}	78.84	65.25
SoE	76.22	66.10
iGAT _{SoE}	75.18	66.50

1)}, we use it to construct an ambiguous pair $a = ((\mathbf{x}_i, y_i), (\mathbf{x}_j, y_j))$ as presented in Fig. 1. We select two base models $\mathbf{h}^0, \mathbf{h}^1 \in \mathcal{H}$ such that \mathbf{h}^0 classifies \mathbf{x}_i well and \mathbf{h}^1 classifies \mathbf{x}_j well. W.l.o.g, let $\mathbf{h} = \mathbf{h}^0$. For the classifiers \mathbf{h}, \mathbf{h}^0 and \mathbf{h}^1 , we analyze the 0-1 loss defined in Eq. (4). Then, we have

$$\begin{aligned} \hat{\mathcal{R}}_{0/1}(a, \max(\mathbf{h}^0, \mathbf{h}^1)) &= \frac{1}{2} (1 [\max(0.9, 0.37) < \max(0.1, 0.63)] \\ &\quad + 1 [\max(0.89, 0.36) < \max(0.11, 0.64)]) = 0, \\ \hat{\mathcal{R}}_{0/1}(a, (\mathbf{h}^0 + \mathbf{h}^1) / 2) &= \frac{1}{2} (1 [(0.9 + 0.37) / 2 < (0.1, 0.63) / 2] \\ &\quad + 1 [(0.89 + 0.36) / 2 < (0.11 + 0.64) / 2]) = 0, \\ \hat{\mathcal{R}}_{0/1}(a, \mathbf{h}) &= \frac{1}{2} (1 [0.9 < 0.63] + 1 [0.36 < 0.64]) = 0.5. \end{aligned}$$

Hence, it has $\hat{\mathcal{R}}_{0/1}(a, \max(\mathbf{h}^0, \mathbf{h}^1)) < \hat{\mathcal{R}}_{0/1}(a, \mathbf{h})$ and $\hat{\mathcal{R}}_{0/1}(a, (\mathbf{h}^0 + \mathbf{h}^1) / 2) < \hat{\mathcal{R}}_{0/1}(a, \mathbf{h})$, which matches the resulting inequality in Theorem 4.1.

11 Additional Experiments and Results

Extra Black-box Attacks: We conduct more experiments to test the effectiveness of iGAT, by evaluating against another two time-efficient and commonly used black-box attacks, using the CIFAR-10 dataset. Results are reported in Table 4. It can be seen that, in most cases, a robustness improvement has been achieved by the enhanced defence.

Varying Perturbation Strengths: In addition to the perturbation strength $\epsilon = 8/255$ tested in the main experiment, we compare the defense techniques under AutoAttack with different settings of perturbation strength. Table 5 reports the resulting classification accuracies, demonstrating that the

Table 5: Comparison of the ensemble robustness (%) to adversarial attacks of various perturbation strengths, using the AutoAttack on CIFAR-10. The results are averaged over five independent runs.

		ϵ				
		2/255	4/255	6/255	8/255	10/255
CIFAR10	CLDL	71.16	60.36	48.89	37.06	26.00
	iGAT _{CLDL}	72.69	61.19	49.07	37.12	25.96
	DVERGE	76.01	64.80	51.92	39.22	27.72
	iGAT _{DVERGE}	76.19	65.14	52.52	39.48	28.59
	ADP	71.93	59.53	47.27	35.52	25.01
	iGAT _{ADP}	76.02	64.76	52.44	40.38	29.46
CIFAR100	SoE	46.55	33.89	23.77	15.92	10.49
	iGAT _{SoE}	45.72	33.18	23.28	16.09	10.52
	DVERGE	48.87	35.81	25.35	17.26	11.18
	iGAT _{DVERGE}	49.43	37.11	26.78	18.60	12.13
	ADP	45.67	33.90	24.42	17.36	12.27
	iGAT _{ADP}	46.33	34.33	24.85	17.86	12.53

Table 6: Comparison between iGAT_{ADP} (average combiner) and a baseline single classifier, evaluated using CIFAR-10 data and the PGD attack ($\epsilon = 8/255$). The results are averaged over five independent runs.

	Natural (%)	PGD (%)	Model size
Single Classifier	81.23	38.33	43M
iGAT _{ADP}	84.95	46.25	9M

Table 7: Probabilities of base models classifying correctly adversarial examples from the CIFAR-10.

	ADP	iGAT _{ADP}	DVERGE	iGAT _{DVERGE}	CLDL	iGAT _{CLDL}
p	41.92%	45.98%	46.25%	47.82%	50.37%	51.02%

Table 8: Distributions of predicted scores by base models correctly classifying adversarial examples from the CIFAR-10.

Interval	<0.5	0.5-0.6	0.6-0.7	0.7-0.8	0.8-0.9	0.9-1.0
iGAT _{ADP}	43.55%	13.30%	11.15%	10.20%	10.62%	11.19%
iGAT _{DVERGE}	20.07%	13.15%	12.20%	12.46%	14.44%	27.69%
iGAT _{CLDL}	49.50%	14.12%	12.26%	13.53%	9.77%	0.81%

Table 9: Expectations of the maximum predicted scores on incorrect classes among base models when tested on adversarial examples from the CIFAR-10.

ADP	iGAT _{ADP}	DVERGE	iGAT _{DVERGE}	CLDL	iGAT _{CLDL}
0.390	0.323	0.476	0.396	0.320	0.281

proposed iGAT is able to improve the adversarial robustness of the studied defense techniques in most cases.

Comparison Against Single Classifiers: To observe how an ensemble classifier performs with specialized ensemble adversarial training, we compare iGAT_{ADP} based on the average combiner against a single-branch classifier. This classifier uses the ResNet-18 architecture, and is trained using only the standard adversarial training without any diversity or regularization driven treatment. Table

Table 10: Probabilities of $h_{y_{\mathbf{x}}}^i(\mathbf{x}) \geq \frac{1-h_{\hat{y}}^i(\mathbf{x})}{C-1}$ for $y_{\mathbf{x}} \neq \hat{y}$ when tested on adversarial examples from the CIFAR-10.

ADP	iGAT _{ADP}	DVERGE	iGAT _{DVERGE}	CLDL	iGAT _{CLDL}
68.74%	73.12%	78.99%	80.19%	78.39%	80.87%

Table 11: Predicted scores on incorrectly classified adversarial examples by the best-performing base model using the CIFAR-10.

ADP	iGAT _{ADP}	DVERGE	iGAT _{DVERGE}	CLDL	iGAT _{CLDL}
0.264	0.291	0.231	0.240	0.235	0.241

6 reports the results. It can be seen that the specialized ensemble adversarial training technique can significantly improve both the natural accuracy and adversarial robustness.

Experiments Driven by Assumption 4.4: To approximate empirically the probability p that a trained base classifier can correctly classify a challenging example, we generate a set of globally adversarial examples $\tilde{\mathbf{X}}$ by attacking the ensemble \mathbf{h} (average combiner) using the PGD and then estimate p on this dataset by $p = \mathbb{E}_{i \in [N], (\mathbf{x}, y_{\mathbf{x}}) \sim (\tilde{\mathbf{X}}, \mathbf{y})} \mathbb{1}[h_{y_{\mathbf{x}}}^i(\mathbf{x}) > \max_{c \neq y_{\mathbf{x}}} h_c^i(\mathbf{x})]$. From Table 7, we can see that all the enhanced ensembles contain base models with a higher probability for correct classifications.

We then examine the distributions of predicted scores by base models when classifying correctly the globally adversarial data generated in the same as in Table 7. It can be seen that the case exists, where a base model correctly classifies a challenging example with a sufficiently large predicted score.

Next, we compute the quantity, i.e., the largest incorrectly predicted score $\mathbb{E}_{i \in [N], (\mathbf{x}, y_{\mathbf{x}}) \sim (\tilde{\mathbf{X}}, \mathbf{y})} \max_{c \neq y_{\mathbf{x}}} h_c^i(\mathbf{x})$, to indirectly estimate whether the small-incorrect-prediction condition, i.e., $f_c(\mathbf{x}) \leq \frac{1-f_{\hat{y}}(\mathbf{x})}{C-1}$ in Assumption 4.4, can be satisfied better after enhancement. Note that $y_i \neq \hat{y}_i$ indicates the incorrect classification while $y_i = \hat{y}_i$ indicates the opposite, both of which are uniformly measured by the defined quantity. This quantity, which is expected to be small, can also be used to evaluate the effect of the proposed regularization term in Eq. (15) on the training. Table 9 shows that the largest wrongly predicted scores by the base models have significantly dropped for all the enhanced ensemble models.

Note that small values of $h_{c \neq y_{\mathbf{x}}}^i(\mathbf{x})$ is equivalent to the high values of $h_{y_{\mathbf{x}}}^i(\mathbf{x})$, and in the theorem, when $\hat{y} \neq y_{\mathbf{x}}$, $h_{y_{\mathbf{x}}}^i(\mathbf{x}) \geq \frac{1-h_{\hat{y}}^i(\mathbf{x})}{C-1}$ is the actual condition expected to be satisfied. Therefore, to examine the second item (the case of misclassification) in Assumption 4.4, we measure the probability $\mathbb{E}_{i \in [N], (\mathbf{x}, y_{\mathbf{x}}) \sim (\tilde{\mathbf{X}}, \mathbf{y})} \mathbb{1}\left[h_{y_{\mathbf{x}}}^i(\mathbf{x}) \geq \frac{1-h_{\hat{y}}^i(\mathbf{x})}{C-1}\right]$ instead. Table 10 shows that after enhancement, the probability of satisfying the condition increases.

As shown in Figure 1, as long as the peaks of two curves are above the line $x = 0.5$ and at similar heights (in which case, are 0.89 and 0.90), whether their height are changed slightly to a higher or lower position will not increase the 0-1 loss. Elevating the low predicted scores to the same level as the high scores serves the crucial factor in fulfilling the cooperative function. Hence, we choose to examine the effect of our distributing rule by checking whether the predicted scores by the best-performing base models on incorrectly classified examples have been increased after enhancement, using the quantity $\mathbb{E}_{(\mathbf{x}, y_{\mathbf{x}}) \sim (\tilde{\mathbf{X}}, \mathbf{y}), \hat{y}_{\mathbf{h}}(\mathbf{x}) \neq y_{\mathbf{x}}} [\max_{i \in [N]} h_{y_{\mathbf{x}}}^i(\mathbf{x})]$. It can be seen from Table 11 that base models were kept improved on the examples they are already good at classifying.

Time Efficiency of iGAT: (1) On distributing rule: We expect the distributing rule to reduce the training data size to $\frac{1}{N}$ for training each base classifier, where N is the number of base classifiers, and therefore to improve the training time. We add an experiment by comparing the training time on $N = 1000$ training samples required by a full version of iGAT_{ADP} and that by a modified version with this distributing rule removed. CIFAR-10 data is used for Evaluation. The observed time for iGAT_{ADP} without the distributing design is 5.63 seconds, while with the distributing design is 5.42 seconds, indicating a slightly reduced training time. (2) On overall training: We illustrate the training

epochs between the ADP defense and its enhancement $iGAT_{ADP}$. ADP necessitates 691 epochs for ADP, whereas $iGAT_{ADP}$ only requires 163 epochs. Based on these, we can conclude that $iGAT_{ADP}$ trains faster than ADP.

Observation of Curvature: We investigated empirically the value of the network curvature $\tilde{\lambda}$ using neural networks trained by the ADP defense techniques, and recorded a $\tilde{\lambda}$ value around 0.06. The smaller value of $\tilde{\lambda}$ indicates a looser upper bound in Eq. (10). According to our Definition 4.3, a looser upper bound allows to define an ambiguous pair containing two intra-class examples that are less close to each other, thus less challenging to classify.